UNIVERSITÀ DEGLI STUDI DI PADOVA

Dipartimento di Fisica e Astronomia "Galileo Galilei"

Master Degree in Physics

Final Dissertation

Electron mass effects in the prediction of muon-electron scattering cross sections

Thesis supervisor

Dr. Massimo Passera

Candidate

Martina Cottini

Academic Year 2020/2021

Acknowledgements

Throughout my academic career I have received a great support from many people and I would like to spend few words to thank them all.

First I would like to thank my supervisor, Dr. Massimo Passera, for his patience, guidance and support. Thanks to him I could work on a very fascinating project. His approach to research and science is a source of inspiration.

I acknowledge Dr. Alessandro Broggio whose availability and expertise was essential to complete this project.

I would like to thank PhD student Elisa Balzani for her patience and availability and for helping me in completing this thesis project.

I special thanks goes to my parents and brother who always support me and my decisions, starting from the choice of my course of study. They have always been there for me. I will never stop thanking them for letting me get here.

I would like to thank my closest friends Chiara and Francesca. They have been by my side since we were children, both in good and bad times. Even though we have lived far away for several years, our friendship has not change but rather it gets much stronger. I can always count on them.

I would like to acknowledge my cousins Beatrice, Micol and Cecilia for listening to my outbursts and for all the unforgettable moments. Before being my cousins they are my great friends.

I would like to acknowledge my colleagues and great friends Annachiara, Elena, Alessandro and Davide with whom I shared my entire university career. It is thanks to them that I have overcome the most difficult moments.

A thank you goes to my roommates Daria, Elena and Luca which made my experience as a transfer student unforgettable. They made living together a fantastic adventure and they became great friends of mine.

Finally, I dedicate this success to myself, to my sacrifices and tenacity that have allowed me to get here.

Contents

Chapter 1

Introduction

The muon anomalous magnetic moment, a_μ or muon "g-2", is one of the most precisely measured quantities in particle physics and allows to test Quantum Field Theory (QFT) in its depth, with unprecedented accuracy. With its electromagnetic, weak and strong interaction contributions, the theoretical prediction of the anomalous magnetic moment of the muon is a very difficult quantity to compute. The comparison between the theoretical and experimental results of the muon"g-2" sets severe limits on the deviations from standard theory of elementary particles, the Standard Model (SM), and, at the same time, opens a window to New Physics (NP). Indeed the present discrepancy between measurement and SM prediction of a_μ is one of the most intriguing hints of NP beyond the SM.

On the experimental side, before April 2021, the experimental value was the one obtained at the E821 experiment at the Brookhaven National Laboratory (BNL). The discrepancy between the BNL measurement and the theoretical SM result was 3.7 σ [1]. In April, the new experimental result of the Muon "g-2" experiment at Fermilab (FNAL) confirmed the BNL result, bringing the combined BNL+FNAL difference between the experimental and SM results to [2,3]

$$a_\mu(\text{Exp}) - a_\mu(\text{SM}) = (251 \pm 59) \times 10^{-11}, \tag{1.1}$$

with a significance of 4.2 σ, if the leading hadronic contribution is computed via the dispersion method. The discrepancy is reduced if the recent BMW collaboration lattice QCD result [4] is employed. In addition, a completely new low-energy approach to measuring the muon "g-2" is being developed by the E34 collaboration at J-PARC [5]. Moreover, in the future, the Muon "g-2" experiment at Fermilab is expected to improve its precision by a factor four. On the theory side, new approaches are being developed in order to reduce the uncertainty of the SM prediction, which is dominated by the hadronic correction.

The long-standing discrepancy between the experimental measurement and the SM prediction of the muon anomalous magnetic moment, a_μ, has kept the hadronic corrections under close scrutiny for several years. In fact, the hadronic uncertainty dominates that of the SM value and is comparable with the experimental one. The leading order hadronic contribution to the muon "g-2", a_μ^{HLO}, is usually computed via a dispersion integral using hadronic production cross sections in electron-positron annihilation at low energies. An alternative theoretical result comes from lattice QCD computations which, however, shows a tension with the dispersive one. The difference deserves further investigation. It is clear that, in order to solve all the discrepancies associated to the muon "g-2", new approaches, both theoretical and experimental, are necessary.

A few years ago a new approach has been proposed to determine the leading hadronic contribution to the muon "g-2", a_μ^{HLO}, measuring the effective electromagnetic coupling $\Delta\alpha(q^2)$, for space-like squared four momentum transfers $q^2 = t < 0$, via scattering data [6]. The elastic scattering of high-energy muons on atomic electrons has been identified as an ideal process for this measurement, leading to the proposal of the MUonE experiment at CERN to extract $\Delta\alpha(q^2)$ from the muon-electron scattering

differential cross section [7]. In order to obtain a result competitive with the dispersive one, the shape of the muon-electron scattering differential cross section must be measured with a systematic uncertainty of $\mathcal{O}(10^{-5})$, or better, close to the kinematic endpoint. An analogous precision is therefore required in the theoretical prediction of the shape of the differential cross section.

The MUonE experiment aims at measuring the running of the coupling constant α in the space-like region with a muon beam of E_μ= 150 GeV on a fixed electron target. Assuming a 150 GeV muon beam with an average intensity of $\sim 1.3 \times 10^7$ muons/s, presently available at CERN's North Area, incident on a target consisting of forty Beryllium layers, each 1.5 cm thick, and two/three years of data taking with the running time of 2×10^7 s/yr, one can reach an integrated luminosity of about $1.5 \times 10^7 \text{nb}^{-1}$. Taking into account the process cross section and the above value of the integrated luminosity, it was estimated that one can reach a statistical sensitivity of roughly 0.3% on the value of a_μ^{HLO} [7].

On the theory side, in order to obtain a theoretical result which can be compared with the one measured at MUonE, leading order (LO), next-to-leading order (NLO) and next-next-to-leading order (NNLO) QED corrections to the differential cross section have to be considered, together with the hadronic ones at NNLO. Until recently, the SM prediction of the $\mu e \to \mu e$ process had received little attention. Only the NLO QED corrections to the differential cross section were computed (long time ago) in [8–14] and revisited in [15]. An important step forward was taken more recently by the authors of [16], who calculated the full set of NLO QED corrections without any approximation and developed a fully differential Monte Carlo code. They also computed the full set of NLO electroweak corrections.

The complete QED corrections at NNLO, crucial to interpret the high-precision data of future experiments like MUonE, are not yet known. A first step towards the calculation of the full NNLO QED corrections to μe scattering was taken in [17–19], where the master integrals for the two-loop planar and non-planar four-point Feynman diagrams were computed. These integrals were calculated setting the electron mass to zero, while retaining full dependence on the muon one. The extraction of the leading electron mass effects from the massless μe scattering amplitudes has been addressed in [20] (see also [21–23]). First applications of Monte Carlo simulations for μe scattering at NNLO have been tested using a subset of two-loop graphs, not yet including the four-point diagrams, with complete dependence on the lepton masses [24,25]. The analytic evaluation of the renormalized two-loop amplitudes for $\mu e \to \mu e$ scattering in QED, with massless electrons and massive muons, has been presented very recently in [26]. The two-loop hadronic corrections to μe scattering were computed in [27,28]. Possible contaminations from New Physics effects were studied in [29,30]. For a comprehensive review of the current theoretical knowledge of the muon-electron scattering cross section for MUonE kinematical conditions we refer the reader to [31].

A new method to compute the QED NNLO correction, based on the expansion by regions approach, would be desirable. The strategy of regions [32] is a technique which allows one to carry out asymptotic expansions of loop integrals in dimensional regularization around various limits [33]. The expansion is obtained by splitting the integration in different regions and by appropriately expanding the integrand in each case. The expanded integrals obtained by means of the strategy of regions technique are in one-to-one correspondence to the Feynman diagrams of effective field theories regularized in dimensional regularization. We will apply this powerful tool to the NLO QED corrections to the muon-electron scattering cross section, in particular to the vacuum polarization and vertex corrections. The small parameter for which we will expand by applying the strategy of regions is the electron mass m, in particular the ratio $\lambda_R = \frac{m^2}{-t}$. Then we will compare the result obtained by the use of this procedure with the Taylor expansion of the exact result of the vacuum polarization and vertex corrections of the μe scattering.

In this thesis project we will start by reviewing the QED, electroweak and hadronic contributions to the anomalous magnetic moment of the muon, paying particular attention to the numerical calculation of the leading hadronic contribution (Cap. 2). Then we will analyze the muon-electron scattering differential cross section at LO and NLO. Ultraviolet singularities will be regularized via conventional dimensional regularization and UV-finite results are obtained in the on-shell renormalization scheme. Moreover we will introduce the soft-Bremsstrahlung corrections in order to take care of the infrared

divergences (Cap. 3). In Cap. 4 we will apply the expansion by regions method to the amplitude for the muon-electron scattering at NLO in QED and we will compare this result with the one obtained by Taylor expanding the exact result for the muon-electron scattering differential cross section.

Chapter 2

The muon anomalous magnetic moment

The Standard Model (SM) provides a truly basic framework for the properties of elementary particles and allows to make theoretical predictions which may be compared with the experiments. The electron and muon anomalous magnetic moments have a prominent role in basic tests of Quantum Field Theory (QFT) with unprecedented accuracy.

2.1 A brief historical overview

Besides charge, spin, mass and lifetime, leptons have other very interesting properties like the magnetic and the electric *dipole moments*. Classically the dipole moments can arise from either electrical charges or currents. An orbiting particle with electric charge e and mass m exhibits a magnetic dipole moment

$$\boldsymbol{\mu}_L = \frac{e}{2mc}\mathbf{L}, \tag{2.1}$$

where $\mathbf{L} = m\mathbf{r} \times \mathbf{v}$ is the orbital angular momentum. Both electric and magnetic moments contribute to the electromagnetic Hamiltonian of the particle:

$$H = -\boldsymbol{\mu}_m \cdot \mathbf{B} - \boldsymbol{d}_e \cdot \mathbf{E}, \tag{2.2}$$

where $\mathbf{B}$ and $\mathbf{E}$ are the magnetic and electric field strengths and $\boldsymbol{\mu}_m$ and $\mathbf{d}_e$ the magnetic and electric dipole moment operators.
The anomalous magnetic moment is an observable which can be relatively easily studied experimentally from the motion of the lepton in an external magnetic field. In 1925 Goudsmit and Uhlenbeck [34] postulated that the intrinsic angular momentum of the electron was equal to $\frac{1}{2}\hbar$ and that, associated to this spin angular momentum, there is a magnetic dipole moment $\mu_0 = \frac{e\hbar}{2mc}$, the *Bohr magneton*. Usually the magnetic moments are measured in terms of μ_0 and of the *spin operator*, $\mathbf{S} = \frac{\hbar\boldsymbol{\sigma}}{2}$, which replaces the angular momentum operator $\mathbf{L}$:

$$\boldsymbol{\mu}_m = gQ\mu_0\frac{\boldsymbol{\sigma}}{2}, \tag{2.3}$$

where $\sigma_i(i{=}1,2,3)$ are the Pauli spin matrices, Q is the electric charge in units of e and g is the gyromagnetic ratio (g-factor). In the same year, Back and Landé [35], after numerous experimental investigations on the Zeeman effect, concluded that the magnetic moment of the electron $(\mu_{\mathrm{m}})_{\mathrm{e}}$ was consistent with the Goudsmit and Uhlenbeck postulate. In 1927, Pauli formulated the quantum mechanical treatment of the electron spin where g remains a free parameter [36]. In 1928, Dirac presented his relativistic theory and predicted, unexpectedly, g =2 for a free electron [37], twice the value g =1 associated with the orbital angular momentum. In 1947, Nafe, Nelson and Rabi [38] reported an anomalous value by about 0.26% in the hyperfine splitting of hydrogen and deuterium, suggesting a possible anomaly of the magnetic moment of the electron. This bring to the definition of the lepton *anomalous magnetic moment*

$$a_l \equiv \frac{g_l - 2}{2} \text{ where } l = e, \mu, \tau. \tag{2.4}$$

In 1948 Kusch and Foley [39], by studying the hyperfine structure of atomic spectra in a constant magnetic field, presented the first precision determination of the anomalous magnetic moment of the electron a_e=0.00119(5). In the same year, the theoretical result was settled by Schwinger who, by working on the renormalization of QED, predicted the 1-loop QED contribution to the anomalous magnetic moment [40]

$$a_l^{\mathrm{QED}(1)} = \frac{\alpha}{2\pi} = 0.00116... \tag{2.5}$$

This contribution is due to quantum fluctuation via virtual electron photon interactions and is universal for all leptons in QED. These theoretical and experimental results provided one of the first tests of the virtual quantum corrections, called *radiative corrections*, predicted by a relativistic QFT.

2.2 The muon anomalous magnetic moment

The theoretical computation of the anomalous magnetic moment of the muon, $a_\mu = \frac{g_\mu - 2}{2}$, has been interesting physicists for over 60 years.
On one hand, the anomalous magnetic moment of the electron, a_e, has been computed precisely and its agreement with the experimental result provided one of the early confirmation of QED. Moreover a_e is almost insensitive to strong and weak interactions, provides a stringent test of QED and, until recently, used to led to the most precise determination of the fine-structure constant α. In the future, this observable will play an important role to test physics Beyond the Standard Model (BSM) [41]. On the other hand, the long-standing discrepancy between the theoretical computation and experimental measurement of the anomalous magnetic moment of the muon indicates a_μ as a better candidate to study BSM physics. In fact, before April 2021, the experimental value was the one obtained at the E821 experiment at the Brookhaven National Laboratory (BNL) and the discrepancy between the BNL measurement and the theoretical SM result was 3.7 σ. In April, the new experimental result of the Muon g-2 experiment at FermiLab (FNAL) confirmed the BNL result, increasing the combined BNL+FNAL discrepancy with the the SM result to 4.2 σ, if the leading hadronic contribution is computed via the traditional dispersive method with $e^+e^- \to hadrons$ data (see later). On the other side, the recent BMW collaboration lattice QCD result weakens this discrepancy [4].

The anomalous magnetic moment of the muon, a_μ, allows to investigate all the SM sectors (electromagnetic, weak and strong interactions), providing a great candidate to unveil New Physics (NP) effects. If Λ indicates the scale of NP, the contribution to the anomalous magnetic moment of a lepton l, a_l, is generally proportional to $\frac{m_l^2}{\Lambda^2}$. This leads to a $\left(\frac{m_\mu}{m_e}\right)^2 \sim 4 \times 10^4$ relative enhancement of the sensitivity of the muon versus the electron magnetic moment. Thus the anomalous magnetic moment of the τ would be the best candidate to investigate NP, but the short lifetime of this lepton makes such measurement very difficult at the moment.

In this chapter a review of the theoretical prediction of a_μ in the SM is presented and all the three contributions (QED, electroweak and hadronic) into which a_μ^{SM} is usually split, are analysed. For detailed reviews see [3,42–44].

2.2.1 QED radiative corrections

The largest contribution to the anomalous magnetic moment is of pure QED origin. The QED contribution to the muon g-2 arises only from the interaction of leptons (e, μ, τ) with photons. As a dimensionless quantity, it can be cast in the following general form [45,46]

$$a_\mu^{\mathrm{QED}} = A_1 + A_2\left(\frac{m_\mu}{m_e}\right) + A_2\left(\frac{m_\mu}{m_\tau}\right) + A_3\left(\frac{m_\mu}{m_e}, \frac{m_\mu}{m_\tau}\right), \tag{2.6}$$

where m_e, m_μ and m_τ are the masses of the electron, muon and tau, respectively. The term A_1, arising from diagrams containing only photons and muons, is mass independent and is therefore universal for all three charged leptons. The contribution A_2 is a function of the indicated mass ratios and only shows up if an additional lepton loop of a lepton different from the muon is involved. This requires at least

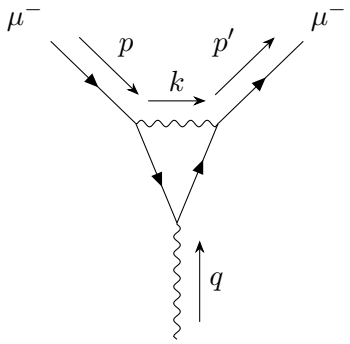

Figure 2.1: QED vertex correction diagram

two more loops: an additional electron loop $A_2\left(m_\mu/m_e\right)$ or an additional τ-loop $A_2\left(m_\mu/m_\tau\right)$. The first produces large logarithms $\propto \ln\left(m_\mu^2/m_e^2\right)$ and accordingly large effects, while the second, because of the *decoupling* of heavy particles in QED like theories, produces only small effects $\propto \left(m_\mu^2/m_\tau^2\right)$. The renormalizability of QED guarantees that the functions A_i can be expanded as a power series in α/π and computed order by order

$$A_i = A_i^{(2)}\left(\frac{\alpha}{\pi}\right) + A_i^{(4)}\left(\frac{\alpha}{\pi}\right)^2 + A_i^{(6)}\left(\frac{\alpha}{\pi}\right)^3 + A_i^{(8)}\left(\frac{\alpha}{\pi}\right)^4 + ... \tag{2.7}$$

One-loop contribution

Only one diagram (fig. 2.1) is involved in the evaluation of the lowest-order contribution and it provides the famous result obtained by Schwinger $A_1^{(2)} = 1/2$.

The Lorentz structure of the vertex correction is given by the three-point function $-ie\Gamma^\mu = \langle\bar{\psi}A^\mu\psi\rangle$, where ψ ($\bar{\psi} = \psi^+\gamma^0$) is the (barred) spinorial representation of the particle, A is the vectorial representation of the photon and e is the electric charge. As a first step we assign a 4-momentum p to the incoming particle, a 4-momentum p' to the outgoing particle and we define the transferred 4-momentum $q \equiv p' - p$ (fig.2.1). This brings to the spinorial representation $u(p)$ for the incoming particle and $\bar{u}(p')$ for the outgoing one. In general Γ^μ is some expression that involves p, p', γ^μ and constants like m and e. We can narrow down the form of Γ^μ by appealing to Lorentz invariance. Since Γ^μ transforms as a vector, it must be a combination of the vectors listed above:

$$-ie\bar{u}(p')\Gamma^\mu u(p) = -ie\bar{u}(p')\left(\gamma^\mu \cdot A + \left(p'^\mu + p^\mu\right)\cdot B + \left(p'^\mu - p^\mu\right)\cdot C\right)u(p), \tag{2.8}$$

where A, B and C are functions of the transferred squared momentum q^2. By applying the Ward identity, $q_\mu\Gamma^\mu = 0$, the only term that does not automatically vanish is the one proportional to C, so C must be zero. The last step is to apply the Gordon identity to obtain

$$-ie\bar{u}(p')\Gamma^\mu(p',p)u(p) = -ie\bar{u}(p')\left(\gamma^\mu F_1(q^2) + \frac{i\sigma^{\mu\nu}q_\nu}{2m}F_2(q^2)\right)u(p), \tag{2.9}$$

where $\sigma^{\mu\nu} = \frac{i}{2}\left[\gamma^\mu,\gamma^\nu\right]$ is the spin 1/2 angular momentum tensor, while F_1 and F_2 are unknown functions of q^2 called *form factors*. In the static limit ($q^2 \to 0$) we have

$$F_1(0) = 1 \text{ and } F_2(0) = a_l. \tag{2.10}$$

The first condition is the *charge renormalization condition*, while the second relation is the finite prediction of the anomalous magnetic moment of the lepton l.

In order to prove the relation $F_2(0) = a_l$, let us analyze the scattering of a particle, like the muon, with a static vector potential $A_\mu^{cl}(x) = (0, \mathbf{A}^{cl}(\mathbf{x}))$. Then the amplitude for scattering from this field is

$$i\mathscr{M} = +ie\left[\bar{u}(p')\left(\gamma^i F_1(q^2) + \frac{i\sigma^{i\nu}q_\nu}{2m}F_2(q^2)\right)u(p)\right]\tilde{A}_{cl}^i(\mathbf{q}). \tag{2.11}$$

The expression in brackets vanishes at $\mathbf{q}$=0, so we must extract from it a contribution linear in q^i. To do this, insert the non relativistic expansion of the spinor $u(p)$:

$$u(p) = \begin{pmatrix} \sqrt{p\cdot\sigma}\xi \\ \sqrt{p\cdot\bar{\sigma}}\xi \end{pmatrix} \approx \sqrt{m}\begin{pmatrix} (1-\mathbf{p}\cdot\boldsymbol{\sigma}/2m)\xi \\ (1+\mathbf{p}\cdot\boldsymbol{\sigma}/2m)\xi \end{pmatrix}, \tag{2.12}$$

and use the identity $\sigma^i\sigma^j = \delta^{ij} + i\epsilon^{ijk}\sigma^k$ to obtain

$$\begin{aligned} \bar{u}(p')\gamma^i u(p) &= 2m\xi'^{\dagger}\left(\frac{-i}{2m}\epsilon^{ijk}q^j\sigma^k\right)\xi, \\ \bar{u}(p')\left(\frac{i}{2m}\sigma^{i\nu}q_\nu\right)u(p) &= 2m\xi'^{\dagger}\left(\frac{-i}{2m}\epsilon^{ijk}q^j\sigma^k\right)\xi. \end{aligned} \tag{2.13}$$

Thus the complete term linear in q^j in the muon-photon vertex function is

$$\bar{u}(p')\left(\gamma^\mu F_1(q^2) + \frac{i\sigma^{\mu\nu}q_\nu}{2m}F_2(q^2)\right)u(p) \underset{q\to 0}{\approx} 2m\xi'^{\dagger}\left(\frac{-i}{2m}\epsilon^{ijk}q^j\sigma^k\left[F_1(0)+F_2(0)\right]\right)\xi. \tag{2.14}$$

Inserting this expression in the eq. 2.11, we find

$$i\mathscr{M} = -i(2m)\cdot e\xi'^{\dagger}\left(\frac{-1}{2m}\sigma^k\left[F_1(0)+F_2(0)\right]\right)\xi\tilde{B}^k(\mathbf{q}), \tag{2.15}$$

where $\tilde{B}^k(\mathbf{q}) = -i\epsilon^{ijk}q^i\tilde{A}^j_{cl}(\mathbf{q})$ is the Fourier transform of the magnetic field produced by $\mathbf{A}^{cl}(\mathbf{x})$. We can interpret $\mathscr{M}$ as the Born approximation to the scattering of the muon from a potential well. The potential is that of a magnetic moment interaction

$$V(\mathbf{x}) = -\langle\boldsymbol{\mu}\rangle\cdot\mathbf{B}(\mathbf{x}), \tag{2.16}$$

where

$$\langle\boldsymbol{\mu}\rangle = g\left(\frac{e}{2m}\right)\mathbf{S} = \frac{e}{m} = 2 + 2F_2(0)\xi'^{\dagger}\frac{\boldsymbol{\sigma}}{2}\xi. \tag{2.17}$$

The magnetic moment of the muon can be rewritten in the standard form

$$\boldsymbol{\mu} = g_\mu\left(\frac{e}{2m}\right)\mathbf{S}, \tag{2.18}$$

where $\mathbf{S}$ is the muon spin and

$$g_\mu = 2\left[F_1(0)+F_2(0)\right] = 2 + 2F_2(0) \quad \Rightarrow a_\mu = F_2(0) = \frac{g_\mu - 2}{2}. \tag{2.19}$$

Now we can evaluate explicitly the one-loop contribution to the muon vertex function. We assign the particle momenta as shown in fig. 2.1 and by applying the Feynman rules listed in App.A, we obtain

$$\bar{u}(p')\Gamma^\mu(p,p')u(p) = -ie^2\int\frac{d^4k}{(2\pi)^4}\bar{u}(p')\frac{\gamma^\nu(\not{q}+\not{k}+M)\gamma^\mu(\not{k}+M)\gamma_\nu}{[(k-p)^2+i\epsilon][(q+k)^2-M^2+i\epsilon][(k^2-M^2)+i\epsilon]}u(p), \tag{2.20}$$

where the $+i\epsilon$ terms in the denominator are necessary for proper evaluation of the loop-momentum integral.

This integral can be computed using the Feynman parameters technique: squeeze the three denominator factors of eq. 2.20 into a single quadratic polynomial in k, raised to the third power; shift k by a constant to complete the square in this polynomial and evaluate the remaining spherically symmetric integral. The price to pay is the introduction of auxiliary parameters to be integrated over. After some lengthy calculation we obtain

$$\begin{aligned} \bar{u}(p')\Gamma^\mu(p,p')u(p) = &-ie^2\int\frac{d^4l}{(2\pi)^4}\int_0^1 dxdydz\delta(x+y+z-1)\frac{2}{D^3} \\ &\times\bar{u}(p')\left[\gamma^\mu\cdot\left(-\frac{1}{2}l^2+(1-x)(1-y)q^2+(1-4z+z^2)M^2\right)\right. \\ &\left.+\frac{i}{2M}\sigma^{i\nu}q_\nu(2M^2z(1-z))\right]u(p), \end{aligned} \tag{2.21}$$

where $D = l^2 - \Delta + i\epsilon$ and $\Delta = -xyq^2 + (1-z)^2 M^2$.
The decomposition into form factors is now manifest and in particular, after performing the integration in d^4l we obtain

$$F_2(q^2) = \frac{\alpha}{2\pi} \int_0^1 dxdydz\delta(x+y+z-1) \left[\frac{2m^2 z(1-z)}{m^2(1-z)^2 - xyq^2} \right] + \mathcal{O}(\alpha^2). \tag{2.22}$$

Now, to obtain the muon anomalous magnetic moment, we have to set $q^2 = 0$ and we get

$$\begin{aligned} a_\mu = F_2(0) &= \frac{\alpha}{2\pi} \int_0^1 dxdydz\delta(x+y+z-1) \left[\frac{2m^2 z(1-z)}{m^2(1-z)^2} \right] \\ &= \frac{\alpha}{\pi} \int_0^1 dz \int_0^{1-z} dy \frac{z}{1-z} = \frac{\alpha}{2\pi}. \end{aligned} \tag{2.23}$$

Higher-order contributions

The QED contribution to the muon g-2 is computed very precisely up to five-loops. Here we will list briefly the results.
At forth order in QED there are seven diagrams that contribute to $A_1^{(4)}$, one to $A_2^{(4)}(m_\mu/m_e)$ and one to $A_2^{(4)}(m_\mu/m_\tau)$. The universal contribution comes from the six diagrams where two virtual photons are attached to the external muon legs and the diagram containing the photon vacuum polarization due to the muon loop. The result has been known for almost 50 years [47, 48]:

$$A_1^{(4)} = -0.328\,478\,965\,579... \tag{2.24}$$

The mass dependent parts come from the two diagrams containing the photon vacuum polarization due to the electron and tau loops. The evaluation of $A_2^{(4)}(m_\mu/m_e)$ and $A_2^{(4)}(m_\mu/m_\tau)$ yields [3]

$$\begin{aligned} A_2^{(4)}(m_\mu/m_e) &= 1.094\,258\,3093(76), \\ A_2^{(4)}(m_\mu/m_\tau) &= 0.000\,078\,076(11), \end{aligned} \tag{2.25}$$

where the standard uncertainties are only caused by the uncertainties of the lepton mass ratios. As there are no two-loop diagrams containing both virtual electrons and taus, $A_3^{(4)}(m_\mu/m_e, m_\mu/m_\tau)$=0.

More then one hundred diagrams are involved in the evaluation of the sixth-order QED contribution. The coefficient $A_1^{(6)}$ arises from 72 diagrams and its calculation in closed analytic form is mainly due to Remiddi and his collaborators [49, 50]

$$A_1^6 = 1.181\,241\,4565... \tag{2.26}$$

The calculation of the exact expression for the coefficient $A_2^{(6)}(m/M)$, where in our case $m = m_\mu$ and $M = m_e$ or m_τ, was completed in 1993 by Laporta e Remiddi [51, 52]. This coefficient can be split into two parts: the first one $A_2^{(6)}(m/M, \mathrm{vp})$ receives contribution from 36 diagrams containing electron or τ vacuum polarization loops [51], whereas the second one $A_2^{(6)}(m/M, \mathrm{lbl})$ is due to 12 light-by-light scattering diagrams with electron or tau loops [52]. The final results are [3]

$$\begin{aligned} A_2^{(6)}(m_\mu/m_e) &= 22.868\,379\,98(20), \\ A_2^{(6)}(m_\mu/m_\tau) &= 0.000\,360\,671(94). \end{aligned} \tag{2.27}$$

The analytic calculation of the three-loop diagrams provides the numerical value [3]

$$A_3^{(6)}(m_\mu/m_e, m_\mu/m_\tau) = 0.000\,527\,738(75). \tag{2.28}$$

More than one thousand diagrams enter the evaluation of the four-loop QED contribution to a_μ. This eight order QED contribution, being about six times larger than the present experimental uncertainty

of a_μ, is crucial for the comparison between the SM prediction of a_μ and its experimental determination. There are 891 four-loop diagrams contributing to the mass independent coefficient $A_1^{(8)}$ and the numerical result is [53]

$$A_1^{(8)} = -1.912\,245\,764. \tag{2.29}$$

The latest values of the coefficient $A_2^{(8)}(m_\mu/m_e)$, arising from 469 diagrams, and the one considering the contribution of the τ lepton are [3]

$$\begin{aligned} A_2^{(8)}(m_\mu/m_e) &= 132.6852(60), \\ A_2^{(8)}(m_\mu/m_\tau) &= 0.042\,4941(53). \end{aligned} \tag{2.30}$$

The three mass coefficient is due to 102 diagrams containing both electron and tau loop insertions [3]

$$A_3^{(8)}(m_\mu/m_e, m_\mu/m_\tau) = 0.062\,722(10). \tag{2.31}$$

The last QED contribution is due to five-loop diagrams. This evaluation is mainly based on the experience accumulated computing the sixth- and eight- order terms. The numerical results for the sum of all diagrams with one or more fermion loops are [3]

$$\begin{aligned} A_2^{(10)}(m_\mu/m_e) &= 742.32(86), \\ A_2^{(10)}(m_\mu/m_\tau) &= -0.0656(45), \\ A_3^{(10)}(m_\mu/m_e, m_\mu/m_\tau) &= 2.011(10). \end{aligned} \tag{2.32}$$

Considering all the QED contributions listed above and the currently best value of the fine structure constant, coming from the electron anomalous magnetic moment a_e [54]

$$\alpha^{-1}(a_e) = 137.035\,999\,1496(13)(14)(330), \tag{2.33}$$

the value for the QED contribution to the muon g-2 is [3]

$$a_\mu^{\mathrm{QED}} = 116\,584\,718.842(7)(17)(6)(100)(28)[106] \times 10^{-11}, \tag{2.34}$$

where the uncertainties are due to the τ-lepton mass m_τ, the eighth-order QED, the tenth-order QED, the estimate twelfth-order QED, the fine-structure constant α and the sum in quadrature of all of these.

2.2.2 Electroweak contribution

The electroweak contribution to the anomalous magnetic moment of the muon is suppressed by a factor $(m_\mu/M_W)^2$, where M_W is the mass of the W boson, with respect to the QED contributions.

One-loop contribution

The one-loop electroweak contribution to the muon g-2 is due to diagrams shown in fig. 2.2 and its analytic form is

$$a_\mu^{EW}(1-loop) = \frac{5G_\mu m_\mu^2}{24\sqrt{2}\pi^2}\left[1 + \frac{1}{5}(1-4\sin^2\theta_W)^2 + \mathcal{O}\left(\frac{m_\mu^2}{M_{Z,W,H}^2}\right)\right], \tag{2.35}$$

where $G_\mu = 1.16637(1) \times 10^{-5}\mathrm{GeV}^{-2}$ is the Fermi coupling constant, M_Z, M_W and M_H are the masses of the Z, W and Higgs boson respectively, while θ_W is the Weinberg angle. The numerical result is [3]

$$a_\mu^{EW}(1-loop) = 194.79(1) \times 10^{-11} \tag{2.36}$$

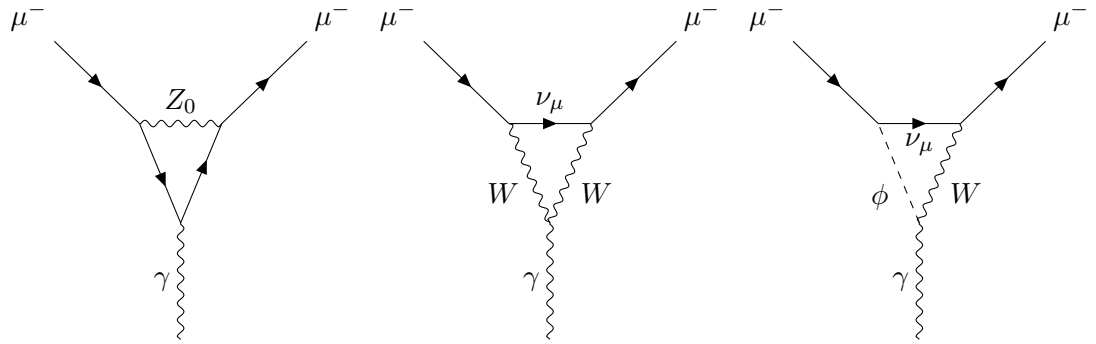

Figure 2.2: Diagrams involved in the computation of the weak contribution at one-loop to the muon g-2

Higher-order contributions

The two-loop electroweak contribution to a_μ [55, 56] leads to a significant reduction of the one-loop prediction. This contribution appeared to be of fundamental importance [57] and, the correction turned out to be enhanced by a factor $\ln(M_{Z,W}/m_f)$, where m_f is a fermion mass scale much smaller then M_W. In QED, loops with three photons attached to a loop do not contribute due to the Furry's theorem and the $\gamma\gamma\gamma$-amplitude vanishes. In presence of weak interactions, because of parity violation, contributions from the two orientations of the closed fermion loops do not cancel such that the $\gamma\gamma Z$, γZZ and γWW amplitudes do not vanish. The two-loop contributions to a_μ^{EW} is usually split into a fermionic and a bosonic part: the first one includes all the two-loop EW corrections containing closed fermion loops, whereas all other contributions are grouped into the second one.

Summing up all the results, the electroweak contribution to the muon g-2 is [3]

$$a_\mu^{EW} = 153.6(1.0) \times 10^{-11}. \tag{2.37}$$

2.2.3 Hadronic contribution

In this section we will analyze the contribution to the muon g-2 arising from QED diagrams involving hadrons. The main effect comes from the $\mathcal{O}(\alpha^2)$ hadronic vacuum polarization (HVP) insertion in the internal photon line of the leading one-loop muon vertex diagram (fig. 2.3). At order $\mathcal{O}(\alpha^3)$, there are

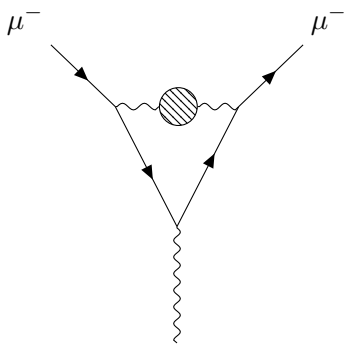

Figure 2.3: HLO contribution to the muon anomalous magnetic moment

several diagrams that contribute to the computation of the anomalous magnetic moment of the muon but with a smaller result. However, these contributions are important if one takes into account the present accuracy of a_μ measurements.

Leading-order hadronic contribution

The hadronic leading order (HLO) contribution to the anomalous magnetic moment of the muon, a_μ^{HLO}, is due to the vacuum polarization correction to the internal photon propagator of the one-loop diagram (fig. 2.3).

The computation of this contribution involves low-energy QCD for which the perturbative approach can not be applied. A different approach to perform this evaluation was found by Bouchiat and Michel [58]: using analyticity and unitarity, $a_\mu^{\rm HLO}$ can be computed from hadronic e^+e^- annihilation data via the dispersion integral [58, 59].

Let us now investigate more in detail the analyticity concept: an analytic function $f(z)$, which has a brunch cut along the real positive axis in the z-plane, starting at $z = z_0$ and going to infinity, and real below z_0, can be written in terms of a Cauchy integral representation

$$f(z) = \frac{1}{2\pi i} \oint_\gamma \frac{f(z')}{z' - z} dz', \tag{2.38}$$

where γ is the contour shown in fig. 2.4. Now let us suppose that $f_1(z)$ is an analytic function defined

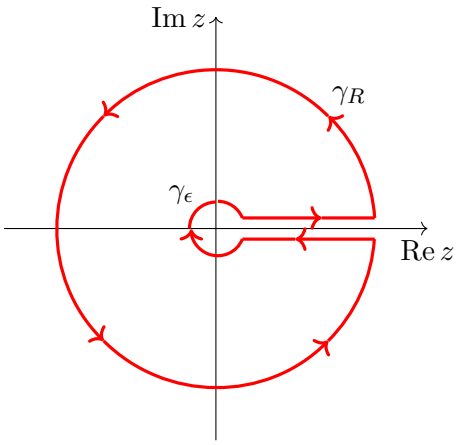

Figure 2.4: Integration path

for complex z in the upper-half z-plane ($Im(z) > 0$); then the Schwarz reflection principle affirms that it exists a unique analytic continuation of $f_1(z)$ in the lower-half z-plane, given by the function $f_2(z) = f_1^*(z^*)$, where * indicates the complex conjugation. Now, if we consider the integration path $z > z_0$, we have

$$f(z) = \frac{1}{2\pi i} \int_{z_0}^{\infty} \frac{f^+(z') - f^-(z')}{z' - z} dz', \tag{2.39}$$

where $f^+(z') = f(z' + i0)$ and $f^-(z') = f(z' - i0)$. From the Schwarz reflection principle we have $f(z' - i\epsilon) = f^*(z' - i\epsilon)$ and so $\lim_{\epsilon \to 0^+} f(z' + i\epsilon) - f(z' - i\epsilon) = 2iIm\,[f(z' + i0)]$.
Considering now the complete integration path (fig. 2.4)

$$f(z) = \frac{1}{2\pi i} \int_{z_0}^{\infty} \frac{2iIm\,[f(z')]}{z' - z} dz' + \frac{1}{2\pi i} \int_{\gamma_\epsilon, \gamma_R} \frac{f(z')}{z' - z} dz'. \tag{2.40}$$

If $f(z)$ falls off sufficiently rapidly in the limit $\epsilon \to 0$ and $R \to \infty$, then the contribution from γ_ϵ and γ_R vanish, and we obtain the *dispersion relation* (DR)

$$f(z) = \frac{1}{\pi} \int_{z_0}^{\infty} \frac{Im\,[f(z')]}{z' - z} dz'. \tag{2.41}$$

If the contribution of γ_R does not vanish, we may subtract the function $f(a)$ from $f(z)$, were a is a regular point of $f(z)$, and let the integral vanish faster at infinity via a factor $\propto 1/z'$:

$$f(z) - f(a) = \frac{z - a}{2\pi i} \int_{z_0}^{\infty} \frac{2iIm\,[f(z')]}{(z' - a)(z' - z)} dz' + \frac{z - a}{2\pi i} \int_{\gamma_\epsilon, \gamma_R} \frac{f(z')}{(z' - a)(z' - z)} dz'. \tag{2.42}$$

Now, if the contribution of γ_R vanishes, we obtain the *subtracted dispersion relation* (SDR):

$$f(z) - f(a) = \frac{z - a}{\pi} \int_{z_0}^{\infty} \frac{Im\,[f(z')]}{(z' - a)(z' - z)} dz'. \tag{2.43}$$

As said before, the hadronic leading order contribution comes from the insertion of the HVP to the internal photon line in the one-loop muon vertex. This correction can be computed by using the dispersion relation for an analytic function just defined. In fact the analyticity of the HVP correction, $\Pi_h(q^2)$, where q^2 is the momentum of the internal photon line, is granted by causality. However we know that $\Pi_h(q^2)$ presents a ultraviolet (UV) divergence, so we have to apply the SDR with a=0 and we obtain

$$\Pi_h(q^2) - \Pi_h(0) = \frac{q^2}{\pi}\int_{4m_\pi^2}^{\infty} \frac{Im\Pi_h(s)}{s(s-q^2)}ds, \tag{2.44}$$

where s is the well known Mandelstam variable. From now on we will use the notation $\bar{\Pi}_h(q^2) \equiv \Pi_h(q^2) - \Pi_h(0)$ for brevity.

Unitarity also implies the validity of the *optical theorem* thanks to which it is possible to relate $Im\Pi_h(s)$ with the experimentally measured cross section. In fact this theorem states that the imaginary part of a forward elastic scattering ($a + b \to a + b$) amplitude arises from a sum of contributions from all possible intermediate state particles ($a + b \to anything$). Up to now, the LO HVP contribution is computed using the cross section for low-energy hadronic e^+e^- annihilation, and this gives the relation

$$Im\Pi_h(s) = \frac{s}{4\pi\alpha}\sigma(e^+e^- \to hadrons) = \frac{\alpha}{3}R(s), \tag{2.45}$$

where $R(s) = \frac{\sigma(e^+e^-\to hadrons)}{4\pi\alpha(s)^2/3s}$, which is obtained by experimental measurement and can not be computed in perturbation theory. The factor at denominator, namely $4\pi\alpha(s)^2/3s$, is the $e^+e^- \to \mu^+\mu^-$ three level cross section, computed in the relativistic limit $s >> 4m_\mu^2$, used as normalization factor. Then the SDR for the LO HVP correction reads

$$\bar{\Pi}_h(q^2) = \frac{\alpha q^2}{3\pi}\int_{4m_\pi^2}^{\infty} \frac{R(s)}{s(s-q^2)}ds. \tag{2.46}$$

With this approach it is possible to compute the LO hadronic correction to the anomalous magnetic moment of the muon without facing the low-energy QCD problems.

The LO hadronic contribution to a_μ is due to the insertion of an hadronic "bubble" in the internal photon propagator of the muon vertex correction (fig. 2.3). So we have to investigate more in details how the photon propagator change with this correction. In the *Feynman gauge*, ξ=1, the free propagator takes the simple form

$$iD^{\mu\nu}(q^2) = \frac{-ig^{\mu\nu}}{q^2 + i\epsilon}. \tag{2.47}$$

By $U(1)_{em}$ gauge invariance, the photon propagator is necessarily massless and must stay massless after including radiative corrections. The transverse part of the full photon propagator becomes

$$iD^{\mu\nu}(q) = \frac{-ig^{\mu\nu}}{q^2(1 + \bar{\Pi}(q^2))} + gauge\, terms. \tag{2.48}$$

where $\bar{\Pi}(q^2)$ is the renormalized vacuum polarization function satisfying the condition $\Pi(0) = 0$. This is a very important result for the study of the LO HVP correction. In fact the equation for the photon propagator (eq. 2.48) can be rewritten as

$$iD^{\mu\nu}(q) = \frac{-ig^{\mu\nu}}{q^2(1 + \bar{\Pi}(q^2))} = \frac{-ig^{\mu\nu}}{q^2}\left[1 - \bar{\Pi}(q^2) + \left(\bar{\Pi}(q^2)\right)^2 + ...\right]. \tag{2.49}$$

So the insertion of the hadronic bubble in the internal photon line leads to the straightforward substitution in the photon propagator:

$$\frac{-ig^{\mu\nu}}{q^2} \to \frac{-ig^{\mu\nu}\left[\Pi_h(0) - \Pi_h(q^2)\right]}{q^2}, \tag{2.50}$$

where we have already performed the subtraction of $\Pi_h(0)$ from $\Pi_h(q^2)$ in order to take care of the UV divergence and we recall the definition $\bar{\Pi}_h(q^2) = \Pi_h(q^2) - \Pi_h(0)$.

We notice that the q^2 dependence on the integral in eq. 2.46 shows up only in the last term. Thus, the free photon propagator in the one-loop vertex diagram is replaced by

$$\frac{-ig^{\mu\nu}}{q^2} \to \frac{-ig^{\mu\nu}}{q^2 - s}, \tag{2.51}$$

which represents the exchange of a photon with "squared mass" s.

Now we have to consider the vertex correction diagram with the insertion of the hadronic vacuum polarization in the internal photon line and, by recalling the expression for the form factor $F_2(0)$ given in eq. 2.22, we obtain

$$F_2(q^2) = \frac{\alpha}{2\pi} \int \frac{ds}{s} \frac{1}{\pi} Im\bar{\Pi}_h(s) \int_0^1 dxdydz\delta(x+y+z-1) \left[\frac{2m^2 z(1-z)}{m^2(1-z)^2 - xyq^2 + zs} \right] + \mathcal{O}(\alpha^2). \tag{2.52}$$

By computing the integral in $dxdydz$, we obtain the positive kernel function

$$K(s) = \frac{\alpha}{\pi} \int_0^1 dx \frac{x^2(1-x)}{x^2 + (1-x)(s/m_\mu^2)}, \tag{2.53}$$

and the muon anomalous magnetic moment is given by

$$a_\mu^{\mathrm{HLO}} = F_2(0) = \frac{\alpha}{\pi^2} \int \frac{ds}{s} Im\bar{\Pi}_h(s) K(s) = \frac{\alpha^2}{3\pi^2} \int \frac{ds}{s} R(s) K(s). \tag{2.54}$$

With this dispersive approach it is possible to overcome the issues involving non-perturbative QCD computations appearing in the LO hadronic contribution to a_μ. The ratio $R(s)$, or equivalently $Im\Pi(s)$, are obtained from low-energy e^+e^- annihilation data, which involves a positive squared momentum transfer and so this is called *time-like* approach.

The latest result for the HLO contribution is [3]:

$$a_\mu^{\mathrm{HLO}} = 6931(40) \cdot 10^{-11}, \tag{2.55}$$

where the error is mainly due to experimental measurement of hadronic e^+e^- annihilation. This *time-like* approach solves the long-distance QCD problems but it suffers from the experimental uncertainties associated to the hadronic e^+e^- annihilation data.

An alternative evaluation of a_μ^{HLO} con be obtained by lattice QCD calculations [3]. The latest result by the BMW collaboration is [4]

$$a_\mu^{\mathrm{HLO}} = 7075(23)(50)\,[5.5] \cdot 10^{-11}. \tag{2.56}$$

Few years ago, a new approach has been proposed to determine the leading hadronic contribution to the muon g-2, measuring the effective electromagnetic coupling in the *space-like* region via scattering data [6]. This leads to the proposal of a new experiment, MUonE at CERN, to measure the differential cross section of muon-electron elastic scattering as a function of the space-like squared momentum transfer $q^2 = t < 0$. This new experiment will use the 150 GeV anti-muon beam already available at CERN and a low-Z target. The differential cross section of that process provides direct sensitivity to the LO hadronic contribution to a_μ. If we now consider the t-channel process described by the muon-electron elastic scattering, and we define the space-like squared four momentum as

$$t(x) = \frac{x^2 m_\mu^2}{x-1} < 0, \tag{2.57}$$

eq. 2.54 reads

$$a_\mu^{\mathrm{HLO}} = F_2(0) = \frac{\alpha}{\pi^2} \int_0^1 dx(1-x) \int \frac{ds}{s} Im\bar{\Pi}_h(s) \frac{-t(x)}{s - t(x)}. \tag{2.58}$$

By recalling the dispersion relation for the hadronic vacuum polarization $\bar{\Pi}_h(q^2)$ (eq. 2.46) and by imposing $q^2 = t(x) < 0$ we obtain [60]

$$a_\mu^{\rm HLO} = \frac{\alpha}{\pi}\int_0^1 dx(x-1)\bar{\Pi}_h[t(x)]. \tag{2.59}$$

This expression of a_μ can be written by considering the effective fine-structure constant at squared momentum q^2. By recalling the form of the dress photon propagator in eq. 2.48 and by including a factor e^2, we obtain

$$iD_\gamma^{\mu\nu}(q) = \frac{-ig^{\mu\nu}e^2}{q^2(1+\bar{\Pi}(q^2))} + gauge\ terms. \tag{2.60}$$

This defines the so called *charge renormalization* condition for which we obtain a running electric charge given by

$$e^2 \to e^2(q^2) = \frac{e^2(0)}{1+[\Pi(q^2)-\Pi(0)]}. \tag{2.61}$$

The full effect of replacing the tree-level photon propagator with the exact photon propagator is therefore to replace

$$\alpha \to \alpha(q^2) = \frac{\alpha(0)}{1+[\Pi(q^2)-\Pi(0)]} = \frac{\alpha(0)}{1-\Delta\alpha(q^2)}, \tag{2.62}$$

where $\Delta\alpha(q^2) = -Re\bar{\Pi}(q^2)$. At this stage it is easy to replace $\bar{\Pi}(q^2) \to \bar{\Pi}_h[t(x)]$ which is the quantity needed to compute the HLO contribution to a_μ. Moreover, for $q^2 = t(x) < 0$, $Im\bar{\Pi}_h[t(x)] = 0$ and eq. 2.59 reads

$$a_\mu^{\rm HLO} = \frac{\alpha}{\pi}\int_0^1 dx(x-1)\Delta\alpha_h[t(x)] \tag{2.63}$$

The hadronic contribution $\Delta\alpha_h[t(x)]$ can be obtained by subtracting from $\Delta\alpha[t(x)]$ the leptonic contribution $\Delta\alpha_{lep}[t(x)]$, which may be computed order by order in perturbation theory.

Higher-order hadronic contributions

The $\mathcal{O}(\alpha^3)$ contribution to the muon g-2 can be divided into two parts:

$$a_\mu^{\rm HHO} = a_\mu^{\rm HHO}({\rm vp}) + a_\mu^{\rm HHO}({\rm lbl}). \tag{2.64}$$

The first term comes from diagrams containing hadronic vacuum polarization insertions into the internal photon line; the second term is the light-by-light contribution. The results considering the hadronic vacuum polarization insertions, $a_\mu^{\rm HHO}({\rm vp})$, were computed both at NLO and NNLO, whereas the light-by-light contribution is computed at LO and NLO [3]:

$$\begin{aligned} a_\mu^{\rm NLO}({\rm vp}) &= -9.83(7)\times 10^{-10},\\ a_\mu^{\rm NNLO}({\rm vp}) &= 1.24(1)\times 10^{-10},\\ a_\mu^{\rm LO}({\rm lbl}) &= 92(19)\times 10^{-11},\\ a_\mu^{\rm NLO}({\rm lbl}) &= 2(1)\times 10^{-11}. \end{aligned} \tag{2.65}$$

2.2.4 SM prediction versus experimental measurement results

On the theory side, the latest result for the muon g-2 obtained considering all the contributions listed above is [3]

$$a_\mu^{\rm SM} = 116\,591\,810(43)\times 10^{-11}. \tag{2.66}$$

This result is obtained by computing the leading hadronic contribution via the traditional dispersive method. An alternative result is obtained by lattice QCD computation thanks to the recent BMW collaboration [4] and reads

$$a_\mu^{\rm lattice} = 116\,591\,954(55)\times 10^{-11}. \tag{2.67}$$

On the experimental side, the measurement of the anomalous magnetic moment of negative muons was the one obtained by the E821 experiment at the Brookhaven National Laboratory (BNL) [1]:

$$a_{\mu^-}^{\text{exp}} = 116\,592\,140(80)(30) \times 10^{-11}, \tag{2.68}$$

where the first error is statistical while the second is systematic. This result is in good agreement with the average of the measurements of the muon g-2 of positive muons [1], $a_{\mu^+}^{\text{exp}} = 116\,592\,030(80) \times 10^{-11}$, as predicted by the CPT theorem. By combining these results, the new average is

$$a_{\mu}^{\text{exp}} = 116\,592\,080(60) \times 10^{-11} \quad (0.5\,\text{ppm}). \tag{2.69}$$

The comparison between the experimental measurement (eq. 2.69) and the SM prediction shows a discrepancy of $3.7\,\sigma$.

On April 2021, the FermiLab Muon g-2 experiment revealed a new experimental result for the anomalous magnetic moment of positive muons [2]:

$$a_{\mu}(\text{FNAL}) = 116\,592\,040(54) \times 10^{-11} \quad (0.46\,\text{ppm}). \tag{2.70}$$

This result differs from the SM value by $3.3\,\sigma$ and agrees with the BNL E821 result. The combined experimental average (BNL+FNAL) is

$$a_{\mu}^{\text{exp}} = 116\,592\,061(41) \times 10^{-11} \quad (0.35\,\text{ppm}). \tag{2.71}$$

The difference, $a_{\mu}^{\text{exp}} - a_{\mu}^{\text{SM}} = (251 \pm 59) \times 10^{-11}$, has a significance of $4.2\,\sigma$.

The long-standing discrepancy between the experimental measurement and the SM prediction makes clear that new approaches, both theoretical and experimental, are necessary. This leads to the proposal of the MUonE experiment at CERN with the aim of measuring the effective electromagnetic coupling $\Delta\alpha(q^2)$ by measuring the muon-electron scattering differential cross section with a systematic uncertainty of $\mathcal{O}(10^{-5})$.

Chapter 3

The muon-electron scattering

The elastic scattering of muons and electrons is one of the most basic process in particle physics. The study of the collision of muons from cosmic rays with atomic electron led to the discovery of the muon. However few experimental results are available for this process. In the 1960s, the first result of the muon-electron elastic scattering cross section came from the experiments at CERN and Brookhaven where accelerator-produced muons were used [61–63]. In the 1990s, the scattering of muons off polarized electrons was used by the SMC collaboration at CERN as a polarimeter for high-energy muon beams.

3.1 Kinematics

The muon-electron elastic scattering is a standard 2→2 process where the masses involved are M for the muon and m for the electron. In our computation we will not make any massless approximation. In order to study this process we label the momentum of the incoming electron with p_1 and the momentum of the incoming muon as p_2; for the outgoing particles we assign the momentum p_3 to the electron and p_4 to the muon. Following this notation the Mandelstam variables read

$$\begin{aligned} s &= (p_1 + p_2)^2 = (p_3 + p_4)^2, \\ t &= (p_1 - p_3)^2 = (p_2 - p_4)^2, \\ u &= (p_1 - p_4)^2 = (p_2 - p_3)^2, \\ s + t + u &= 2m^2 + 2M^2. \end{aligned} \tag{3.1}$$

We are interested in the differential cross section for the μe elastic scattering whose general expression is

$$d\sigma = \frac{|\bar{\mathscr{M}}|^2}{4I_{12}}(2\pi)^2\delta^4(p_1 + p_2 - p_3 - p_4)\frac{d^3p_3}{(2\pi)^3 2E'_e}\frac{d^3p_4}{(2\pi)^3 2E'_\mu}, \tag{3.2}$$

where $I_{12} = \sqrt{(p_1 \cdot p_2)^2 - m^2M^2}$, $E'_e = \sqrt{m^2 + |\mathbf{p_3}|^2}$ is the electron recoil energy and $E'_\mu = \sqrt{M^2 + |\mathbf{p_4}|^2}$ is the energy of the outgoing muon. By integrating in d^3p_4 and by shifting to spherical polar coordinates, $d^3p_3 = |\mathbf{p_3}|^2 d\mathbf{p_3}d\Omega$, we obtain

$$\frac{d\sigma}{d\Omega} = \frac{|\bar{\mathscr{M}}|^2}{4I_{12}}\int \frac{d\mathbf{p_3}}{(4\pi)^2}\frac{|\mathbf{p_3}|^2}{E'_e E'_\mu}\delta(|\mathbf{p_3}| - |\hat{p_3}|)\left|\frac{\partial(E'_e + E'_\mu)}{\partial|\mathbf{p_3}|}\right|^{-1}. \tag{3.3}$$

In the center of mass frame (CoM), from the conservation of energy and momentum, we have the relations

$$\begin{aligned} \sqrt{s} &= E_e + E_\mu = E'_e + E'_\mu, \\ \mathbf{p_1} &= -\mathbf{p_2}, \\ \mathbf{p_3} &= -\mathbf{p_4}, \end{aligned} \tag{3.4}$$

and these lead to the expressions

$$\begin{aligned} &\frac{\partial(E'_e + E'_\mu)}{\partial|\mathbf{p_3}|} = |\mathbf{p_3}|\frac{E'_\mu + E'_e}{E'_\mu E'_e} \\ &I_{12} = |\mathbf{p_3}|\sqrt{s} \end{aligned} \tag{3.5}$$

By integrating in $d\mathbf{p_3}$, we obtain the expression for the differential cross section

$$\frac{d\sigma}{d\Omega} = \frac{|\bar{\mathscr{M}}|^2}{64\pi^2 s}. \tag{3.6}$$

By considering the Mandelstam variable t defined in eq. 3.1, we obtain, in the CoM frame

$$\begin{aligned} t = (p_1 - p_3)^2 = 2m^2 - 2p_1 \cdot p_3 = -2|\mathbf{p_3}|^2(1 - cos\theta) \\ \Rightarrow dt = 2|\mathbf{p_3}|^2 dcos\theta, \end{aligned} \tag{3.7}$$

where θ is the angle between the incoming muon and the emitted electron.
From the conservation of energy and momentum (eq. 3.4) it is possible to prove the relation

$$|\mathbf{p_3}|^2 = \frac{1}{4s}\Lambda(s, M^2, m^2), \tag{3.8}$$

where $\Lambda(x, y, z) = x^2 + y^2 + z^2 - 2xy - 2xz - 2yz$ is the Källen function. So the differential cross section can be rewritten as

$$\frac{d\sigma}{dt} = \frac{|\bar{\mathscr{M}}|^2}{16\pi\Lambda(s, M^2, m^2)}. \tag{3.9}$$

In the laboratory frame, for a fixed target experiment where the electron is initially at rest, the momenta are

$$p_1 = \begin{pmatrix} m \\ 0 \end{pmatrix} \; p_2 = \begin{pmatrix} E_\mu \\ \mathbf{p_2} \end{pmatrix} \; p_3 = \begin{pmatrix} E'_e \\ \mathbf{p_3} \end{pmatrix} \; p_3 = \begin{pmatrix} E'_\mu \\ \mathbf{p_4} \end{pmatrix} \; . \tag{3.10}$$

In this frame of reference, the Mandelstam variables can be rewritten as

$$\begin{aligned} &s = 2mE_\mu + M^2 + m^2, \\ &t = -2m(E'_e - m), \\ &-\Lambda(s, M^2, m^2)/s < t < 0. \end{aligned} \tag{3.11}$$

3.2 LO contribution

In the SM, at LO, there are four diagrams that contribute to the muon-electron scattering cross section and they differ from each other because of the different propagators involved. As shown in fig. 3.1, the propagator can be a photon, a Z-boson, a Higgs boson or a neutral Goldstone boson.

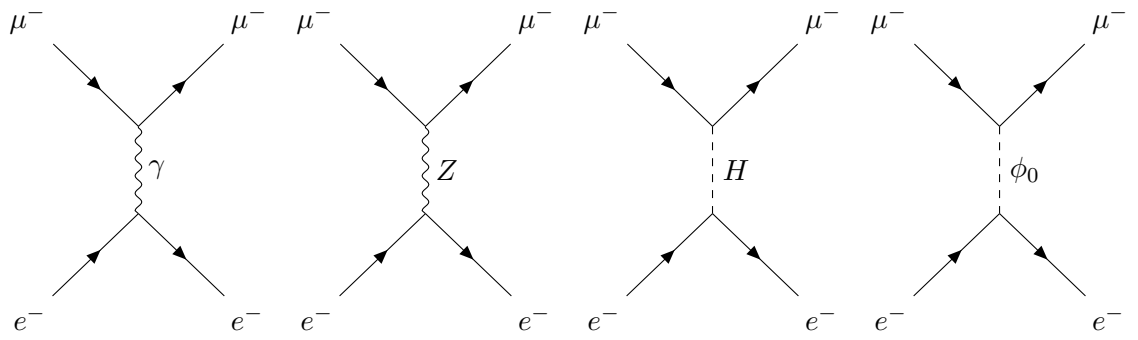

Figure 3.1: LO diagrams for the muon-electron scattering cross section, considering all the possible propagators

The LO amplitude will be the sum of all these contributions and, by labelling $\mathscr{M}_\gamma$, $\mathscr{M}_Z$, $\mathscr{M}_H$ and $\mathscr{M}_{\phi_0}$ the amplitudes involving photon, Z-boson, Higgs boson and neutral Goldstone boson propagators respectively, we obtain

$$\begin{aligned}\mathscr{X}_{LO} &= \frac{1}{4}\sum_{spins}|\mathscr{M}_\gamma + \mathscr{M}_Z + \mathscr{M}_H + \mathscr{M}_{\phi_0}|^2 \\ &= \mathscr{X}_\gamma + \mathscr{X}_Z + \mathscr{X}_H + \mathscr{X}_{\phi_0} + 2\times \sum_{\substack{i,j=\{\gamma,Z,H,\phi_0\}\\ i\neq j}} Re(\mathscr{M}_i\mathscr{M}_j^*),\end{aligned} \tag{3.12}$$

where the $\mathscr{X}_i$ are the squared matrix elements while the last term is the interference between them. The factor $\frac{1}{4}$ comes from the average over the spins of the initial particles. We are interested in a very precise computation of the muon-electron scattering cross section ($\mathcal{O}(\alpha^4)$) and, as the contributions from Z, H and ϕ_0 are of $\mathcal{O}(10^{-5})$, they must be included. Here we will discuss only the QED contribution coming from the interaction of leptons (electron and muon) with the photon.

At LO in QED there is only one diagram with a t-channel exchange of a photon. It is precisely this

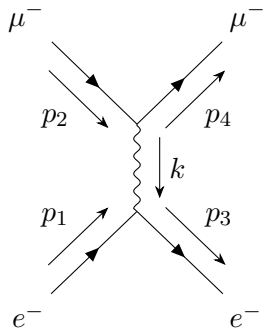

Figure 3.2: LO diagram for the muon-electron scattering cross section, involving the photon propagator

feature that makes this process ideal to extract the HVP. In fact, the dominant contribution to the HVP comes from the insertion of the hadronic vacuum polarization Π_h into the photon propagator.

By considering the diagram in fig. 3.2, the unpolarized Feynman amplitude can be easily computed by applying the rules listed in App. A:

$$\begin{aligned}\mathscr{X}_\gamma &= \frac{1}{4}\sum_{spins}\frac{e^4}{q^4}\bar{u}(p_3)\gamma^\mu u(p_1)\bar{u}(p_4)\gamma_\mu u(p_2)\bar{u}(p_1)\gamma^\nu u(p_3)\bar{u}(p_2)\gamma_\mu(p_4) \\ &= \frac{1}{4}\frac{e^4}{t^2}Tr\left[(\not{p}_3+m)\gamma^\mu(\not{p}_1+m)\gamma^\nu\right]Tr\left[(\not{p}_4+M)\gamma_\mu(\not{p}_2+M)\gamma_\nu\right],\end{aligned} \tag{3.13}$$

where we use the energy-momentum conservation to set $q^2=(p_1-p_3)^2=t$. By computing the traces and by evaluating in the lab frame the scalar products originating from the traces, we obtain the result

$$\mathscr{X}_\gamma = \frac{4e^4}{t^2}\left[(s-m^2-M^2)^2+st+\frac{t^2}{2}\right]. \tag{3.14}$$

The LO cross section for the muon-electron scattering then, from eq. 3.9, reads

$$\frac{d\sigma_0}{dt} = 4\pi\alpha\,\frac{\left[(s-m^2-M^2)^2+st+\frac{t^2}{2}\right]}{t^2\Lambda(s,M^2,m^2)}. \tag{3.15}$$

3.3 NLO contribution

At NLO in QED there are three diagrams that contribute to the muon-electron scattering cross section, the so called *virtual* corrections: the vacuum polarization correction, the vertex correction and the box

diagram. Since we are interested in the $\mathcal{O}(\alpha^3)$ correction to the differential cross section, we have to compute the interference term between this virtual corrections and the LO matrix element $\mathscr{M}_\gamma$:

$$\mathscr{X}_{\rm NLO} = \frac{1}{4}\sum_{spins} 2Re\left[\mathscr{M}_\gamma^* \mathscr{M}_{\rm NLO}\right]. \tag{3.16}$$

All these contributions will be computed in terms of the Passarino-Veltman functions and in the on-shell renormalization scheme.

3.3.1 QED renormalization

The renormalized perturbation theory, formulated in terms of physically measurable parameters, is based on the following steps:

- absorb the field-strength renormalizations into the Lagrangian by rescaling the fields;
- split each term of the Lagrangian into two pieces, absorbing the infinite and unobservable shifts into counterterms;
- specify the renormalization conditions, which define the physical masses and coupling constants and keep the field-strength renormalizations equal to 1;
- compute amplitudes with the new Feynman rules, adjusting the counterterms as necessary to mantain the renormalization conditions.

We will apply this procedure to QED. Let us consider the QED Lagrangian for the electron

$$\mathscr{L}_0 = -\frac{1}{4}F_{\mu\nu}F^{\mu\nu} + \bar{\psi}(i\partial\!\!\!/ - m_0)\psi - e_0\bar{\psi}\gamma^\mu\psi A_\mu, \tag{3.17}$$

where m_0 is the *bare* mass while e_0 is the *bare* electric charge. The electron and photon propagators coming from this Lagrangian are

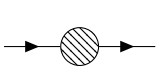
$= \dfrac{iZ_2}{p\!\!\!/ - m} + ...,$ 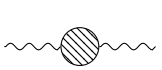
$= \dfrac{-iZ_3 g_{\mu\nu}}{q^2} + ...$ (3.18)

To get rid of the terms Z_2 and Z_3, we have to substitute in the Lagrangian the renormalized fields $\psi = Z_2^{1/2}\psi_r$ and $A^\mu = Z_3^{1/2}A_r^\mu$. Moreover we introduce the physical electric charge e, measured at large distances (q=0), by defining

$$e_0 Z_2 Z_3^{1/2} = eZ_1. \tag{3.19}$$

Then the Lagrangian can be split into two pieces: one which is the so called renormalized QED Lagrangian and the other one depending on counterterms

$$\begin{aligned}\mathscr{L} =& -\frac{1}{4}(F_r^{\mu\nu})^2 + \bar{\psi}_r(i\partial\!\!\!/ - m)\psi_r - e\bar{\psi}_r\gamma^\mu\psi_r A_{r\mu} \\ & -\frac{1}{4}\delta_3(F_r^{\mu\nu})^2 + \bar{\psi}_r(i\delta_2\partial\!\!\!/ - \delta_m)\psi_r - e\delta_1\bar{\psi}_r\gamma^\mu\psi_r A_{r\mu}\end{aligned} \tag{3.20}$$

where $\delta_3 = Z_3 - 1$, $\delta_2 = Z_2 - 1$, $\delta_m = Z_2 m_0 - m$ and $\delta_1 = Z_1 - 1 = (e_0/e)Z_2 Z_3^{1/2} - 1$.
This renormalized Lagrangian implies new Feynman rules:

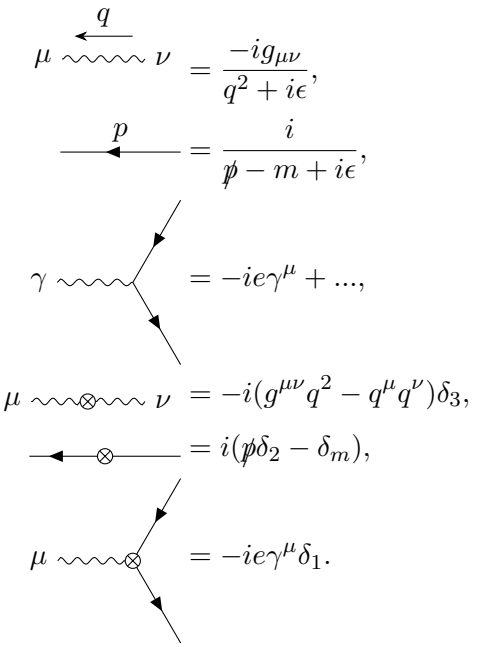

$$
\begin{aligned}
&= \frac{-ig_{\mu\nu}}{q^2 + i\epsilon}, \\
&= \frac{i}{\not{p} - m + i\epsilon}, \\
&= -ie\gamma^\mu + ..., \\
&= -i(g^{\mu\nu}q^2 - q^\mu q^\nu)\delta_3, \\
&= i(\not{p}\delta_2 - \delta_m), \\
&= -ie\gamma^\mu \delta_1.
\end{aligned}
\tag{3.21}
$$

Each of the four counterterm coefficients must be fixed by a renormalization condition:

$$
\begin{aligned}
\Sigma(\not{p} = m) &= 0, \\
\frac{d}{d\not{p}}\Sigma(\not{p})\Big|_{\not{p}=m} &= 0, \\
\Pi(q^2 = 0) &= 0, \\
-ie\Gamma^\mu(p' - p = 0) &= -ie\gamma^\mu,
\end{aligned}
\tag{3.22}
$$

where $\Sigma(\not{p})$ identify the electron self-energy correction. The first condition in eq. 3.22 fixes the electron mass at m, while the next two fix the residues of the electron and photon propagators at 1. The last condition sets the electron charge to be e.

The four conditions in eq. 3.22 allow us to determine the four conterterms in terms of the values of loop diagrams which, at one-loop, are the electron self-energy, the vacuum polarization and the vertex diagrams. The relation necessary to compute the counterterms are

$$
\begin{aligned}
m\delta_2 - \delta_m &= \Sigma(m), \\
\delta_2 &= \frac{d}{d\not{p}}\Sigma(m), \\
\delta_3 &= \Pi(0), \\
\delta_1 &= -F_1(0),
\end{aligned}
\tag{3.23}
$$

where $F_1(q^2)$ is the form factor defined in the computation of the vertex correction (eq. 2.9). We will use dimensional regularization to control ultraviolet divergences while we will introduce a real photon with mass λ to control infrared divergences.

For the analysis of the muon-electron scattering cross section at one-loop, only the vacuum polarization and vertex corrections are UV divergent, so we are interested in the computation of the δ_3 and δ_1 counterterms. By evaluating explicitly these contributions we get

$$
\delta_3(m) = \Pi(0) = -\frac{\alpha}{3\pi}\left(\frac{2}{\epsilon} - \gamma + \ln(4\pi) + \ln\left(\frac{\mu^2}{m^2}\right)\right), \tag{3.24}
$$

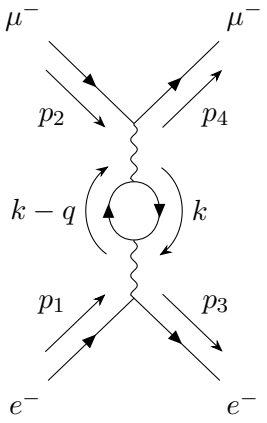

Figure 3.3: Vacuum polarization diagram for the muon-electron scattering cross section

where m could be the mass of the electron, the muon or the tau lepton and $\epsilon = \frac{4-d}{2}$.
For the vertex contribution, instead, the counterterm reads

$$\delta_1(m) = -\frac{\alpha}{4\pi}\left(\frac{2}{\epsilon} - \gamma + \ln(4\pi) + \ln\left(\frac{\mu^2}{m^2}\right) + 2\ln\left(\frac{\lambda^2}{m^2}\right) + 4\right). \tag{3.25}$$

By adding these counterterms to the virtual amplitude we will obtain a UV finite result.

3.3.2 Vacuum polarization contribution

The first virtual correction consists in a tree level diagram with a vacuum polarization insertion into the photon propagator (fig. 3.3). By associating the momenta like in fig. 3.3, the vacuum polarization correction $\Pi(q^2)$ can be computed by applying the Feynman rules listed in App. A in d dimension and by neglecting the external legs

$$\Pi(q^2) = -(e\mu^\epsilon)^2 \int \frac{d^dk}{(2\pi)^d} \frac{Tr\left[\gamma^\mu(\not{k}+m)\gamma^\nu(\not{q}+\not{k}+m)\right]}{(k^2-m^2)\left[(k+q)^2-m^2\right]}, \tag{3.26}$$

where $q = p_1 - p_3$ from the momentum conservation, $d = 4-2\epsilon$, k is the loop momentum and m is the electron mass. We neglect the $+i\epsilon$ prescription for brevity. The muon-electron scattering cross section at one loop feels the contribution of the vacuum polarization correction with a muon or a tau lepton and the amplitude can be computed by considering eq. 3.26 and by substituting $m \to M$ and $m \to m_\tau$ respectively.

This calculation can be carried out both by hand or by the *FeynCalc* package of Mathematica [64–66]. In both cases the result can be expressed in terms of the Passarino-Veltman functions. For the VP contribution the final expression depends on the $B_0(...)$ function which can be divided into a divergent term and a finite term:

$$B_0(...) = \frac{1}{\epsilon} - \gamma_E + \ln(4\pi) + \ln(\mu^2) + fB_0(...), \tag{3.27}$$

where $\gamma_E \simeq 0.577216$ while $fB_0(...)$ denotes the finite part of the Passarino-Veltman function $B_0(...)$. The definitions of all the Passarino-Veltman functions are listed in App. B.

It is clear, from the explicit expression of the $B_0(...)$ functions, that the vacuum polarization contributions shows a UV divergence and in order to eliminate it we have to add to the amplitude the counterterms $\delta_3(m_i)$ (eq. 3.24) where $m_i = \{m, M, m_\tau\}$. Only after considering these counterterms, it is possible to take the $d \to 4$ limit safely.

The UV finite result for the interference term between the VP correction and the LO matrix element

$\mathscr{M}_\gamma$, coming from eq. 3.16, can be represented diagrammatically as

$$\mathscr{M}_{VP} = \frac{1}{4} \times 2Re \left[\left(\right)^* \times \sum_{l=e,\mu,\tau} \left(+ \right) \right] \tag{3.28}$$

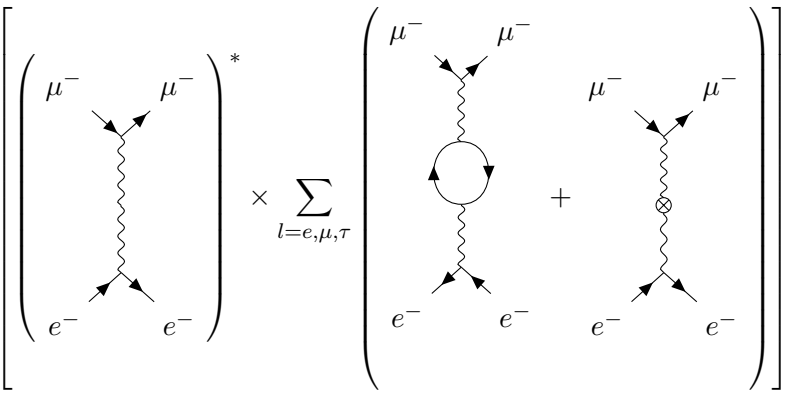

where the sum is meant over an electron, muon or tau vacuum polarization while the diagram with the cross insertion in the photon propagator represents the counterterm necessary to obtain a UV finite result.

The explicit expression for the total VP amplitude reads:

$$\begin{aligned} \mathscr{X}_{VP} = Re\Big[&- \frac{64\pi\alpha^3}{3t^3}(2(m^2+M^2-s)^2+2st+t^2) \sum_{m_i} \Big(b_1(m_i) f B_0(t, m_i^2, m_i^2) \\ &- b_2(m_i) f B_0(0, m_i^2, m_i^2) + 2t \ln(m_i) - t \Big) \Big], \end{aligned} \tag{3.29}$$

where $m_i = \{m, M, m_\tau\}$ while the coefficients $b_1(m_i)$ and $b_2(m_i)$ will be listed in Sec. 3.5.

3.3.3 Vertex contribution

The vertex correction comes from the insertion of a photon propagator between the incoming and outgoing muon or electron (fig. 3.4). In order to compute this diagram we associate the momenta like

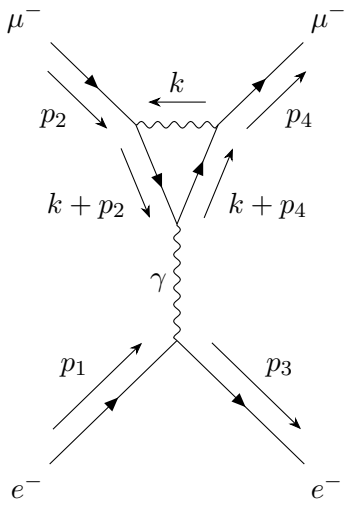

Figure 3.4: Vertex contribution to the muon-electron scattering cross section

in fig. 3.4 and, by making use of the Feynman rules quoted in App. A, we obtain the following integral in d dimension:

$$\bar{u}(p_4)\Gamma^\mu u(p_2) = -ie^2 \int \frac{d^dk}{(2\pi)^d} \frac{\bar{u}(p_4)\gamma^\rho \left[(\not{k}+\not{p}_2+M)\right]\gamma^\mu \left[(\not{k}+\not{p}_4+M)\right]\gamma_\rho u(p_2)}{(k^2-\lambda^2)[(k+p_2)^2-M^2][(k+p_4)^2-M^2]}, \tag{3.30}$$

where λ is a fictitious mass of the photon introduced to regularize the infrared divergences. Also in this case the $+i\epsilon$ prescription has been neglected for brevity. The same vertex correction but for the

electron can be computed starting from eq. 3.30 and by applying the substitutions $M \to m$, $p_2 \to p_1$ and $p_4 \to p_3$.

As for the VP contribution, the computation can be done both by hand or by using the *Feyncalc* package [64–66]. The result will be expressed in terms of the Passarino-Veltman functions, where in addition to the $B_0(...)$ function, for the vertex correction, the final expression will depend on the $C_0(...)$ functions.

This vertex contribution shows both a UV divergence and a IR divergence. The counterterm $\delta_1(m_i)$ where $m_i = \{m, M\}$ (eq. 3.25) is necessary in order to obtain a UV finite result while the IR divergence can be eliminated by considering the *soft-Bremsstrahlung* contribution (see Sec.3.4). Once we have obtained a UV finite result, we can take the $d \to 4$ limit, in analogy with the VP contribution, while the $\lambda \to 0$ limit can be applied only after the introduction of the soft-Bremsstrahlung cross section.

The interference term between the vertex correction and the LO matrix element $\mathscr{M}_\gamma$ (eq. 3.16) is given by

$$\mathscr{M}_V = \frac{1}{4} \times 2Re \left[\left(\right)^* \times \sum_{l=e,\mu} \left(+ \right) \right] \tag{3.31}$$

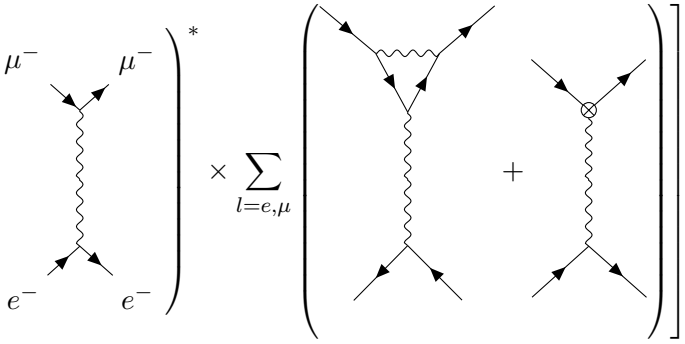

where the sum is meant over an electron and muon vertex while the diagram with the cross insertion is the counterterm necessary to obtain a UV finite result.

The explicit expression of the total vertex amplitude is

$$\begin{aligned} \mathscr{X}_V = Re\Big[& \frac{16\pi\alpha^3}{t^2} (c_1 C_0(M^2, M^2, t, M^2, \lambda^2, M^2) + c_2 C_0(m^2, m^2, t, m^2, \lambda^2, m^2) \\ & + b_3 f B_0(0, M^2, M^2) + b_4 f B_0(t, M^2, M^2) + b_5 f B_0(0, m^2, m^2) + b_6 f B_0(t, m^2, m^2) \\ & + a_1 \ln(\lambda) + a_2 \ln(M) + a_3 \ln(m) + a_4) \Big] \end{aligned} \tag{3.32}$$

where the coefficients c_i $(i = 1, 2)$, b_j $(j = 3, 4, 5, 6)$ and a_k $(k = 1, 2, 3, 4)$ will be listed in Sec. 3.5.

3.3.4 Box contribution

The last virtual contribution is the one which involve the box diagram (fig. 3.5). The first diagram in fig. 3.5 is the *direct* (||) box diagram while the second one is called *crossed* (×) diagram.
The crossed diagram can be obtained from the direct one if we invert the muon line, add an overall minus sign before the crossed diagram and make the substitution $u = 2m^2 + 2M^2 - s - t \to s$. So a very important check for the computation of this diagram is the comparison between the direct and the crossed diagram through the relation

$$= - \quad (u \leftrightarrow s) \tag{3.33}$$

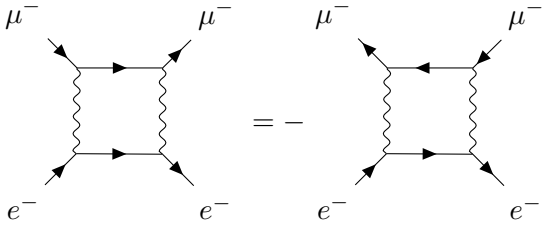

Then the box contribution can be computed by considering the momenta defined in fig.3.5, by applying the Feynman rules listed in App. A and by keeping all the external legs in order to simplify the

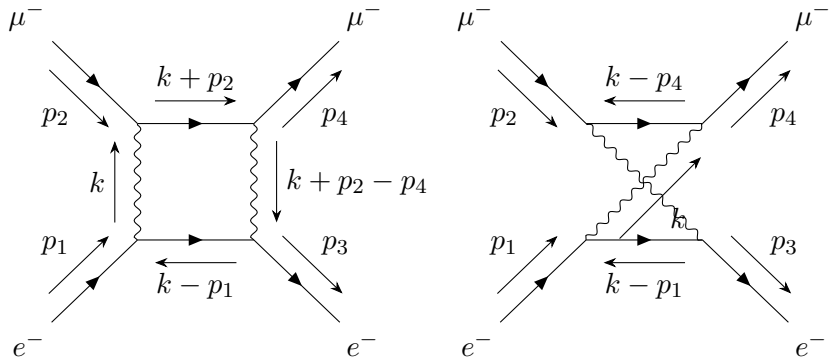

Figure 3.5: Box contribution to the muon-electron scattering cross section

expression thanks to the Dirac equation:

$$\mathscr{M}_B^{||} = e^4 \int \frac{d^dk}{(2\pi)^d} \frac{\bar{u}(p_3)\gamma^\rho\big[-(\not{k}-\not{p}_1)+m\big]\gamma^\sigma u(p_1)\bar{u}(p_4)\gamma_\rho\big[(\not{k}+\not{p}_2)+M\big]\gamma_\sigma u(p_2)}{(k^2-\lambda^2)\big[(k-p_1)^2-m^2\big]\big[(k+p_2)^2-M^2\big]\big[(k+p_2-p_4)^2-\lambda^2\big]}, \tag{3.34}$$

where the $+i\epsilon$ prescription is neglected for brevity. The crossed diagram contribution $\mathscr{M}_B^{\times}$ can be computed from $\mathscr{M}_B^{||}$ by applying the substitution $p_2 \to -p_4$ and $p_4 \to -p_2$ in all the amplitude expression (eq. 3.34) except the spinors.
The box diagram is UV finite, as it is possible to notice from a dimensional analysis, but it is IR divergent so the soft-Bremsstrahlung contribution must be considered. Only after cancelling the IR divergence it is possible to take the $\lambda \to 0$ limit.

In this case the computation was performed only by using the *Feyncalc* package and, in order to use the Dirac equation and contract the Lorentz indices, we first contract the amplitude in eq. 3.34 with the LO one (eq. 3.13) and then we solve the loop integral in terms of the Passarino-Veltman functions. This procedure was possible thanks to the UV finiteness of the box diagram.

In analogy with the VP and vertex corrections, the interference term can be expressed diagrammatically as

$$\mathscr{M}_B = \frac{1}{4} \times 2Re\left[\sum_{||,\times}\left(\begin{array}{c}\mu^- \quad \mu^- \\ \\ e^- \quad e^-\end{array}\right)^* \times \begin{array}{c}\mu^- \quad\quad \mu^- \\ \\ e^- \quad\quad e^-\end{array}\right] \tag{3.35}$$

where the sum is meant on the direct ($||$) and crossed ($\times$) box diagrams.
Eventually the box contribution reads

$$\begin{aligned}\mathscr{X}_B = Re\Bigg[\frac{16\pi\alpha^3}{t}\Big(& d_1 D_0(m^2,m^2,M^2,M^2,t,s,\lambda^2,m^2,\lambda^2,M^2) \\ &+ d_2 D_0(m^2,m^2,M^2,M^2,t,u,\lambda^2,m^2,\lambda^2,M^2) + c_3 C_0(m^2,m^2,t,\lambda^2,m^2,\lambda^2) \\ &+ c_4 C_0(M^2,M^2,t,\lambda^2,M^2,\lambda^2) + c_5 C_0(m^2,M^2,s,m^2,\lambda^2,M^2) \\ &+ c_6 C_0(m^2,M^2,u,m^2,\lambda^2,M^2) + b_7 fB_0(0,m^2,m^2) + b_8 fB_0(0,M^2,M^2) \\ &+ b_9 fB_0(s,m^2,M^2) + b_{10} fB_0(t,0,0) + b_{11} fB_0(u,m^2,M^2) + a_5\Big)\Bigg].\end{aligned} \tag{3.36}$$

where the coefficients d_l $(l=1,2)$, c_i $(i=3,4,5,6)$, b_j $(j=7,8,9,10,11)$ and a_5 will be listed in Sec. 3.5.

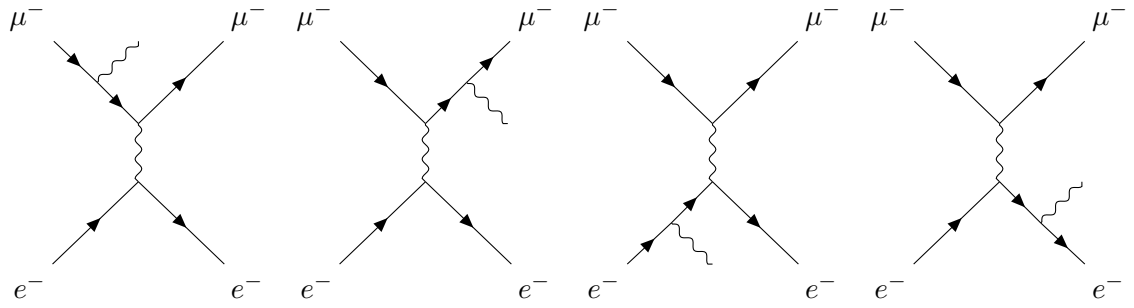

Figure 3.6: Bremsstrahlung contribution for the muon-electron scattering cross section

3.4 Soft-Bremsstrahlung contribution

In the previous section we saw that the vertex and the box corrections to the virtual amplitude for the muon-electron scattering show a IR divergence when $\lambda \to 0$, that can be cured by the introduction of the soft-Bremsstrahlung contribution.

The Bremsstrahlung correction is given by diagrams like the ones in fig. 3.6 where a photon is radiated from an initial or final muon or electron. So we will end up with four diagrams, one for every external legs which radiate a photon. With the term *soft* we indicate the fact that we are considering photons with an energy less than some specified value ω_0. This threshold energy ω_0 may coincide with the sensitivity threshold of the experimental set up. Here the computation of this contribution will be performed by hand following the approach applied by G. t' Hooft and M. Veltman [67].

As a first step we identify with $k = (k_0, \mathbf{k})$, where $|\mathbf{k}| < k_0$, the 4-momentum of the radiated soft photon and with λ its fictitious mass. Then the amplitude is given by

$$\mathscr{X}_{soft} = -\mathscr{X}_\gamma \times e^2 \int_{k_0<\omega_0} \frac{d^3k}{(2\pi)^3 2\omega_0} \left| \mathscr{E}(p_1, p_2, p_3, p_4, k) \right|^2, \tag{3.37}$$

where we have factorized the LO amplitude and

$$\mathscr{E}(p_1, p_2, p_3, p_4, k) = -\frac{p_1}{p_1 \cdot k} - \frac{p_2}{p_2 \cdot k} + \frac{p_3}{p_3 \cdot k} + \frac{p_4}{p_4 \cdot k}. \tag{3.38}$$

We now show the basic steps to obtain the result in eq. 3.37. We consider the case in which a soft photon is radiated from an incoming muon (the first diagram in fig. 3.6); by applying the Feynman rules in App. A, the amplitude reads

$$\mathscr{M}_2 = \frac{(-ie)^3}{t} \bar{u}(p_3)\gamma^\mu u(p_1)\bar{u}(p_4)\gamma_\mu \frac{\not{p}_2 - \not{k} + M}{[(p_2 - k)^2 - M^2]} \gamma^\nu \epsilon^*_\nu(k) u(p_2). \tag{3.39}$$

Since we are considering the soft Bremsstrahlung component, every $\not{k}$ and λ^2 term at numerator is negligible with respect to $\not{p}_2$ and M. Then, by considering the relation $(p_2 - k)^2 - M^2 = -2p_2 \cdot k$, $\mathscr{M}_2$ will be given by

$$\mathscr{M}_2 = \left[\frac{ie^2}{t} \bar{u}(p_3)\gamma^\mu u(p_1)\bar{u}(p_4)\gamma_\mu u(p_2) \right] e \left(-\frac{p_2 \cdot \epsilon^*(k)}{p_2 \cdot k} \right) = \mathscr{M}_\gamma e \left(-\frac{p_2 \cdot \epsilon^*(k)}{p_2 \cdot k} \right). \tag{3.40}$$

Then in order to obtain the squared matrix element we take the absolute value of $\mathscr{M}_2$ and we have to remember that

- the sum over the photon polarization, in the case $\lambda \to 0$, yields: $\sum_{pol} \epsilon^*_\mu(k)\epsilon_\nu(k) = -g_{\mu\nu}$;
- the recoil of the fermion by the emitted photon is neglected;
- the integral over $\mathbf{k}$ shows up as a phase space integral (eq. 3.37).

We obtain similar contributions from the other diagrams in fig. 3.6, which can be derived from $\mathscr{M}_2$ by the substitutions $(p_2 \to p_1)$, $(p_2 \to -p_3, k \to -k)$ and $(p_2 \to -p_4, k \to -k)$.
Once we consider all the contributions, the scalar integrals to compute have the form

$$I(p_i, p_j) = \int_{k_0<\omega_0} \frac{d^3k}{(2\pi)^3 2k_0} \frac{1}{(k \cdot p_i)(k \cdot p_j)} \tag{3.41}$$

where $p_i, p_j = \{p_1, p_2, p_3, p_4\}$.

In the laboratory frame we obtain the following result for the soft-Bremsstrahlung amplitude:

$$\begin{aligned} \mathscr{X}_{soft} = \mathscr{X}_\gamma \times \frac{4\pi\alpha}{2(2\pi)^3} \Bigg[& - m^2 \Big(I(p_1,p_1) + I(p_3,p_3) \Big) + 2\Big(m^2 - \frac{t}{2} \Big) I(p_1,p_3) \\ & - M^2 \Big(I(p_2,p_2) + I(p_4,p_4) \Big) + 2\Big(M^2 - \frac{t}{2} \Big) I(p_2,p_4) \\ & + (m^2 + M^2 - s) \Big(I(p_1,p_2) + I(p_3,p_4) \Big) \\ & + (m^2 + M^2 - u) \Big(I(p_1,p_4) + I(p_2,p_3) \Big) \Bigg] \end{aligned} \tag{3.42}$$

The scalar integrals are computed following the procedure in [67] and the steps of the computations of them are sketched in App. B. The integral with $p_i = p_j$ is easier to compute with respect to the case $p_i \neq p_j$. Moreover it is possible to prove that $I(p_1,p_1) = I(p_3,p_3)$, $I(p_2,p_2) = I(p_4,p_4)$, $I(p_1,p_2) = I(p_3,p_4)$ and $I(p_1,p_4) = I(p_2,p_3)$.

Only some of the C_0 functions and both the D_0 are IR divergent and, thanks to [68, 69], it is possible to write these functions as a sum of a IR divergent part and a IR finite term. Then it is clear which integrals of the soft-Bremsstrahlung cross section (eq. 3.42) cancel the IR divergence of the vertex correction and box diagrams. Here we will show the cancellation of the IR divergences of the one-loop virtual diagrams thanks to an explicit combination of the scalar integrals from the soft-Bremsstrahlung contribution.

- Electron vertex correction

$$\begin{aligned} & Re\Bigg[\frac{16\pi\alpha^3}{t^2} \Big(c_2 C_0(m^2, m^2, t, m^2, \lambda^2, m^2) + a_1 \ln(\lambda) \Big) \Bigg] \\ & + \mathscr{X}_\gamma \times \frac{\alpha}{4\pi^2} \Bigg[- 2m^2 I(p_1,p_1) + 2\Big(m^2 - \frac{t}{2} \Big) I(p_1,p_3) \Bigg] \end{aligned} \tag{3.43}$$

- Muon vertex correction

$$\begin{aligned} & Re\Bigg[\frac{16\pi\alpha^3}{t^2} \Big(c_2 C_0(M^2, M^2, t, M^2, \lambda^2, M^2) + a_1 \ln(\lambda) \Big) \Bigg] \\ & + \mathscr{X}_\gamma \times \frac{\alpha}{4\pi^2} \Bigg[- 2M^2 I(p_2,p_2) + 2\Big(M^2 - \frac{t}{2} \Big) I(p_2,p_4) \Bigg] \end{aligned} \tag{3.44}$$

- Direct box correction

$$\begin{aligned} & Re\Bigg[\frac{16\pi\alpha^3}{t^2} \Big(d_1 D_0(m^2, m^2, M^2, M^2, t, s, \lambda^2, m^2, \lambda^2, M^2) + c_5 C_0(m^2, M^2, s, m^2, \lambda^2, M^2) \Big) \Bigg] \\ & + \mathscr{X}_\gamma \times \frac{\alpha}{4\pi^2} 2(m^2 + M^2 - s) I(p_1,p_2) \end{aligned} \tag{3.45}$$

- Crossed box correction

$$Re\left[\frac{16\pi\alpha^3}{t^2}\Big(d_2 D_0(m^2,m^2,M^2,M^2,t,u,\lambda^2,m^2,\lambda^2,M^2)+c_6 C_0(m^2,M^2,u,m^2,\lambda^2,M^2)\Big)\right] + \mathscr{X}_\gamma \times \frac{\alpha}{4\pi^2}2(m^2+M^2-u)I(p_1,p_4) \tag{3.46}$$

Once we have cancelled all the IR divergences in the vertex and box diagrams we can safely take the $\lambda \to 0$ limit. Moreover we remark that the three-point functions $C_0(m^2,m^2,t,\lambda^2,m^2,\lambda^2)$ and $C_0(M^2,M^2,t,\lambda^2,M^2,\lambda^2)$ in the box amplitude are already IR finite. So, from now on, their arguments λ will be set to zero.

3.5 Total virtual amplitude

The complete virtual amplitude is given by the sum of the vacuum polarization, vertex and box amplitudes obtained in the previous sections. In the on-shell renormalization scheme we obtain a result which is UV finite and it reads

$$\begin{aligned}\mathscr{X}_{virtual} = Re\Bigg[\frac{16\pi\alpha^3}{t}\Big(&v_1 D_0(m^2,m^2,M^2,M^2,t,s,\lambda^2,m^2,\lambda^2,M^2)\\ &+ v_2 D_0(m^2,m^2,M^2,M^2,t,u,\lambda^2,m^2,\lambda^2,M^2) + v_3 C_0(m^2,m^2,t,m^2,\lambda^2,m^2)\\ &+ v_4 C_0(M^2,M^2,t,M^2,\lambda^2,M^2) + v_5 C_0(m^2,m^2,t,0,m^2,0)\\ &+ v_6 C_0(M^2,M^2,t,0,M^2,0) + v_7 C_0(m^2,M^2,s,m^2,\lambda^2,M^2)\\ &+ v_8 C_0(m^2,M^2,u,m^2,\lambda^2,M^2) + v_9 fB_0(0,m^2,m^2) + v_{10} fB_0(0,M^2,M^2)\\ &+ v_{11} fB_0(t,m^2,m^2) + v_{12} fB_0(t,M^2,M^2) + v_{13} fB_0(s,m^2,M^2)\\ &+ v_{14} fB_0(t,0,0) + v_{15} fB_0(u,m^2,M^2) + v_{16} fB_0(t,m_\tau^2,m_\tau^2)\\ &+ v_{17} fB_0(0,m_\tau^2,m_\tau^2) + v_{18}\ln(m) + v_{19}\ln(M) + v_{20}\ln(m_\tau) + v_{21}\ln(\lambda) + v_{22}\Big)\Bigg]\end{aligned} \tag{3.47}$$

For brevity, we left the $\ln(\lambda)$ term in the final expression but we have shown in the previous section that it can be cancelled by the introduction of the soft-Bremsstrahlung contribution, so that we obtain a IR finite result. The explicit expressions of the coefficients are:

- $v_1 = d_1 = -\left((m^2+M^2-s)\left(4\left(m^2+M^2-s\right)^2+2st+t^2\right)\right)$
- $v_2 = d_2 = -\left((m^2+M^2-s-t)\left(4\left(m^2+M^2-s\right)^2-4t\left(m^2+M^2\right)+6st+3t^2\right)\right)$
- $v_3 = \frac{c_1}{t} = \frac{2}{t}\left(2M^2-t\right)\left(2\left(m^2+M^2-s\right)^2+2st+t^2\right)$
- $v_4 = \frac{c_2}{t} = \frac{2}{t}\left(2m^2-t\right)\left(2\left(m^2+M^2-s\right)^2+2st+t^2\right)$
- $v_5 = c_3 = \frac{2\left(-8m^2t+8m^4+t^2\right)\left(2\left(m^2+M^2-s\right)-t\right)}{4m^2-t}$
- $v_6 = c_4 = \frac{2\left(-8M^2t+8M^4+t^2\right)\left(2\left(m^2+M^2-s\right)-t\right)}{4M^2-t}$
- $v_7 = c_5 = -2(2s+t)\left(m^2+M^2-s\right)$
- $v_8 = c_6 = -2\left(4m^2+4M^2-2s-t\right)\left(m^2+M^2-s-t\right)$

- $v_9 = \frac{4}{3t^2}(2(m^2+M^2-s)^2+2st+t^2)b_2(m) + \frac{b_5}{t} + b_7$ where

$$b_5 = \frac{-8t\left(m^2\left(M^2-5s\right)+m^4+\left(M^2-s\right)^2\right)+24m^2\left(m^2+M^2-s\right)^2+8t^2\left(2m^2-s\right)-4t^3}{4m^2-t}$$

$$b_7 = 2m\Bigg(\frac{2mt\left(m^2-M^2-s\right)}{-2m^2\left(M^2+s\right)+m^4+\left(M^2-s\right)^2}+\frac{8m\left(m^2-M^2+s\right)}{t-4m^2} + \frac{(m+M)\left((m-M)^2-s\right)}{(m-M)^2-s-t}+\frac{(m-M)\left((m+M)^2-s\right)}{(m+M)^2-s-t}+2m\Bigg)$$

- $v_{10} = \frac{4}{3t^2}(2(m^2+M^2-s)^2+2st+t^2)b_2(M) + \frac{b_3}{t} + b_8$ where

$$b_3 = \frac{1}{4M^2-t}\Big[-8t\left(m^2\left(M^2-2s\right)+m^4-5M^2s+M^4+s^2\right) + 24M^2\left(m^2+M^2-s\right)^2+8t^2\left(2M^2-s\right)-4t^3\Big]$$

$$b_8 = 2M\Bigg(\frac{2Mt\left(-m^2+M^2-s\right)}{-2m^2\left(M^2+s\right)+m^4+\left(M^2-s\right)^2}+\frac{8M\left(-m^2+M^2+s\right)}{t-4M^2} + \frac{(m+M)\left((m-M)^2-s\right)}{(m-M)^2-s-t}+\frac{(m-M)\left(s-(m+M)^2\right)}{(m+M)^2-s-t}+2M\Bigg)$$

- $v_{11} = -\frac{4}{3t^2}(2(m^2+M^2-s)^2+2st+t^2)b_1(m) + \frac{b_6}{t}$ where

$$b_6 = \frac{4m^2t\left(M^2-7s\right)-16m^2\left(m^2+M^2-s\right)^2+6t^2\left(s-2m^2\right)+6m^4t+6t\left(M^2-s\right)^2+3t^3}{4m^2-t}$$

- $v_{12} = -\frac{4}{3t^2}(2(m^2+M^2-s)^2+2st+t^2)b_1(M) + \frac{b_4}{t}$ where

$$b_4 = \frac{1}{4M^2-t}\Big[2t\left(2m^2\left(M^2-3s\right)+3m^4-14M^2s+3M^4+3s^2\right) - 16M^2\left(m^2+M^2-s\right)^2+6t^2\left(s-2M^2\right)+3t^3\Big]$$

- $v_{13} = b_9 = -\frac{2\left(-m^2\left(2M^2(s+t)+M^4-3s^2\right)+m^4\left(-M^2-3s+t\right)+m^6+t\left(M^4-s^2\right)+\left(M^2-s\right)^3\right)}{-2m^2(M^2+s)+m^4+(M^2-s)^2}$
- $v_{14} = b_{10} = \frac{2(4mM-t)(4mM+t)\left(2\left(m^2+M^2-s\right)-t\right)}{(4m^2-t)(t-4M^2)}$
- $v_{15} = b_{11} = \frac{2}{((m-M)^2-s-t)((m+M)^2-s-t)}\Big[m^2(2M^2(s-4t)+M^4-(3s-t)(s+t)) + m^4(M^2+3s)-m^6+t^2(M^2+s)+2st(s-M^2)-(M^2-s)^3\Big]$
- $v_{16} = -\frac{4}{3t^2}(2(m^2+M^2-s)^2+2st+t^2)b_1(m_\tau)$
- $v_{17} = \frac{4}{3t^2}(2(m^2+M^2-s)^2+2st+t^2)b_2(m_\tau)$
- $v_{18} = -\frac{8}{3t} + \frac{a_3}{t}$ where $a_3 = 6\left(2\left(m^2+M^2-s\right)^2+2st+t^2\right)$
- $v_{19} = -\frac{8}{3t} + \frac{a_2}{t}$ where $a_2 = 6\left(2\left(m^2+M^2-s\right)^2+2st+t^2\right)$
- $v_{20} = -\frac{2}{3t}$

- $v_{21} = \frac{a_1}{t}$ where $a_1 = -16\left(m^2 + M^2 - s\right)^2 - 16st - 8t^2$
- $v_{22} = \frac{4}{3t} + \frac{a_4}{t} + a_6$ where

$$a_4 = \frac{1}{(4m^2 - t)\,(t - 4M^2)}\Bigg[4t\Bigg(- 2t\Big(- 4s(m^2 + M^2) + 6m^2M^2 + m^4 + M^4 + s^2\Big) + 2t^2\Big(2(m^2 + M^2) - s\Big) + 4(m^2 + M^2)((m - M)^2 - s)((m + M)^2 - s) - t^3\Bigg)\Bigg]$$

$$a_5 = 4\Bigg(\frac{8m^2\left(m^2 - M^2 + s\right)}{t - 4m^2} + \frac{2t\left(\left(m^2 - M^2\right)^2 - s\left(m^2 + M^2\right)\right)}{-2m^2\left(M^2 + s\right) + m^4 + \left(M^2 - s\right)^2} + \frac{8M^2\left(-m^2 + M^2 + s\right)}{t - 4M^2} + 2\left(m^2 + M^2\right) + \frac{(m + M)^2\left((m - M)^2 - s\right)}{(m - M)^2 - s - t} + \frac{(m - M)^2\left((m + M)^2 - s\right)}{(m + M)^2 - s - t}\Bigg)$$

where $b_1(m_i) = 2m_i^2 + t$ and $b_2(m_i) = 2m_i^2$.

From the previous section, we obtain the $\mathcal{O}(\alpha^3)$ correction to the differential cross section

$$\frac{d\sigma_{\text{NLO}}}{dt} = \frac{d\sigma_0}{dt} + \frac{\mathscr{X}_{virtual} + \mathscr{X}_{soft}}{16\pi\Lambda(s, M^2, m^2)} \tag{3.48}$$

which is an expression of the masses m^2 and M^2, the Mandelstam variables s and t and of the threshold energy for the experimental set up ω_0, once we have introduced the soft-Bremsstrahlung contribution. In App. B the explicit expression of the Passarino-Veltman functions and the integrals from the soft-Bremsstrahlung contribution are listed.
This result is obtained by considering the scattering of μ^- over e^-. The same computation can be performed for the antiparticles μ^+. This leads to an overall minus sign for the box amplitude, $I(p_1, p_2)$ and $I(p_1, p_4)$, while the vertex and the vacuum polarization contributions remain unchanged.

Chapter 4

Expansion by regions method

As we saw in the previous chapter, the QED corrections at one-loop to the μe elastic scattering amplitude, and consequently the QED differential cross section, are well known. On the contrary the NNLO QED corrections are not known yet so a new method to compute them, based on the expansion by regions approach, would be desirable.

In this chapter we will explain the basic concept under the expansion by regions method and we will apply it to the NLO QED corrections, in particular to the vacuum polarization and vertex corrections. Then we will compare the result obtained by the use of this procedure with the Taylor expansion of the exact result of this two corrections, obtained by standard methods.

4.1 The strategy of regions

The strategy of regions [32] is a technique which allows one to carry out asymptotic expansions of loop integrals in dimensional regularization around various limits [33]. When loop integrals involve many different scales from masses and kinematical parameters, it can be hard to evaluate them exactly. The integrand may be simplified before integration by exploiting hierarchies of the parameters and expanding in powers of small ratios. When this expansion are done naively, neglecting their breakdown in certain parts of the integration domain, new singularities may be generated and important contributions to the full result can be missed. The expansion by regions approach allows to treat this singularities properly.

The general strategy to obtain the expansion of a given Feynman integral in a given kinematic limit is [33]: identify the regions of the integrand which lead to singularities in the given limit; expand the integrand in each region and integrate each expansion over the full phase space; add the result of the integrations over the different regions to obtain the expansion of the original full integral. This method will be successful only if all the expanded integrals are properly regularized in dimensional regularization. Moreover each region has to be considered only once to avoid double counting and the regions defined in the calculations at one loop are often the same which are relevant at higher order.

The expansion by regions method is a very powerful tool because, if one is simply interested in the expansion of some perturbative result in a small parameter, one can therefore work directly with this method, without constructing an effective Lagrangian.

4.2 Muon-electron scattering amplitude expansion

By considering the muon-electron elastic scattering amplitude, the small parameter for which it is applied the expansion by regions method is the electron mass m. In particular we will perform the expansion in terms of the parameter $\lambda_R = \frac{m^2}{-t}$.

We will apply this method to the vacuum polarization and the vertex corrections. The result will be

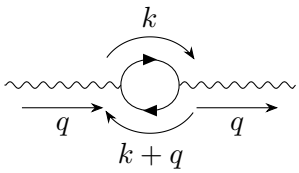

Figure 4.1: $B_0(t, m^2, m^2)$ diagrammatic representation.

UV finite and gauge invariant. In fact, the UV divergences are cured by the introduction of counterterms, so the final expressions in eq. 3.29 and eq. 3.32, to which we will apply the strategy of regions, are UV finite (but not IR finite). We will also obtain a gauge invariant result because, in analogy with the considerations done in [70] for the process $e^+e^- \to \tau^+\tau^-$, the vacuum polarization is gauge-independent by itself; the gauge dependence of the direct box cancels exactly against that of the crossed box; the gauge-dependence of the vertex correction can therefore cancel only against the fermion self-energy graphs renormalizing the external (on-shell) fermions. The application of the expansion by regions method to the box contribution is more complicated with respect to the VP and vertex corrections, due to the four-point function D_0, and it will be discussed in the future. Here the expansion by regions method will be applied to the computation of the gauge-invariant subset given by the electron-line contributions. This approach, in which we neglect the box contribution to the μe scattering amplitude, is justified from an experimental point of view because it is possible to perform the measurement in a kinematic region where the box happens to be numerically sub-leading [16].

During this analysis, the IR divergences will be evaluated in dimensional regularization and they will be left explicit because, as we saw in sec. 3.4, they are cancelled by the soft-Bremsstrahlung contribution whose Taylor expansion in m^2 can be trivially performed.

By looking at the final expression of the VP and vertex corrections (eq. 3.29 and eq. 3.32), the expansion by regions approach can be applied to two Passarino-Veltman functions: $B_0(t, m^2, m^2)$ and $C_0(m^2, m^2, t, m^2, 0, m^2)$ where we set the limit $\lambda \to 0$ for the fictitious photon mass in the C_0 function in order to treat the IR divergences in dimensional regularization.
In the next sections we will sketch the procedure to expand these functions with the strategy of regions.

4.2.1 $B_0(t, m^2, m^2)$

The expansion of the B_0 function is a simple but clear example of how this method works. This function represent the tadpole diagram in fig. 4.1 and it is given by

$$B_0(t, m^2, m^2) = \frac{\mu^{2\epsilon}}{i\pi^2} \int d^d k \frac{1}{(k^2 - m^2)[(k+q)^2 - m^2]}, \tag{4.1}$$

where $q^2 = (p_1 - p_3)^2 = t$, k is the loop momentum and $d = 4 - 2\epsilon$.
Then the scales involved are $q^2 = t$ and m^2 so we can identify three different regions [71] and expand in terms of the parameter $\lambda_R = \frac{m^2}{-t}$.

1. $|k^2| \sim |q^2| >> m^2$ then the denominators in eq. 4.1 become

$$\begin{aligned} (k^2 - m^2) &\sim k^2 \left(1 - \frac{m^2}{k^2} + ...\right), \\ [(k+q)^2 - m^2] &\sim (k+q)^2 \left(1 - \frac{m^2}{(k+q)^2} + ...\right). \end{aligned} \tag{4.2}$$

   So we obtain the integral

$$I_{1,B_0} = \frac{\mu^{2\epsilon}}{i\pi^2} \int d^d k \frac{1}{k^2(k+q)^2} \left(1 + \frac{m^2}{k^2} + ...\right) \left(1 + \frac{m^2}{(k+q)^2} + ...\right). \tag{4.3}$$

By considering only the first term of the expansion, by using the Feynman parameters and by performing the integration in d^dk (App. A.3), we obtain

$$\begin{aligned} I_{1,B_0} &= \frac{\mu^{2\epsilon}}{\pi^\epsilon}\frac{\Gamma(\epsilon)}{(-t)^\epsilon}\int_0^1 dx[(1-x)-(1-x)^2]^{-\epsilon} \\ &= \frac{\mu^{2\epsilon}}{\pi^\epsilon}\frac{\Gamma(\epsilon)}{(-t)^\epsilon}\frac{\Gamma(1-\epsilon)^2}{\Gamma(2-2\epsilon)}. \end{aligned} \tag{4.4}$$

2. $|k^2| \sim m^2$ so the propagator denominators become

$$\begin{aligned} &(k^2-m^2), \\ &[(k+q)^2-m^2] \sim q^2\left(1+\frac{k^2+2k\cdot q-m^2}{q^2}+...\right). \end{aligned} \tag{4.5}$$

and the integral in eq. 4.1 reads

$$I_{2,B_0} = \frac{\mu^{2\epsilon}}{i\pi^2}\int d^dk \frac{1}{(k^2-m^2)q^2}\left(1-\frac{k^2+2k\cdot q-m^2}{q^2}+...\right). \tag{4.6}$$

By applying the steps done in the previous region, the $\mathcal{O}(1)$ contribution is

$$I_{2,B_0} = -\frac{\mu^{2\epsilon}}{\pi^\epsilon}\frac{\Gamma(\epsilon-1)}{t}(-\lambda t)^{-\epsilon}. \tag{4.7}$$

3. $|(k+q)^2| \sim m^2$:

$$\begin{aligned} &(k^2-m^2) \sim -q^2\left(1+\frac{2k\cdot q}{q^2}\right), \\ &[(k+q)^2-m^2]. \end{aligned} \tag{4.8}$$

So

$$I_{3,B_0} = \frac{\mu^{2\epsilon}}{i\pi^2}\int d^dk \frac{1}{[(k+q)^2-m^2](-q^2)}\left(1-\frac{2k\cdot q}{q^2}+...\right), \tag{4.9}$$

The result at $\mathcal{O}(1)$ is equal to the one obtained in the region where $|k^2| \sim m^2$ except for an overall minus sign.

Now we sum all the contributions coming from the regions defined above and we expand for $\epsilon \to 0$ to obtain

$$B_0(t,m^2,m^2) = \Delta - \ln(-t) + 2, \tag{4.10}$$

where $\Delta = \frac{1}{\epsilon} - \gamma - \ln(\pi) + \ln(\mu^2)$. This result is completely consistent with the result obtained by expanding the explicit expression of the $B_0(t,m^2,m^2)$ function evaluated by standard methods, including its UV divergent term.

By considering higher order terms in the computation of the integrals in the different regions, it is possible to check the consistency of the result at $\mathcal{O}(\lambda_R)$ obtained with the strategy of regions:

$$B_0(t,m^2,m^2) = \Delta - \ln(-t) + 2 + 2\lambda_R\left[\ln(\lambda_R)-1\right]. \tag{4.11}$$

The Δ expression identifies the UV divergent part of the $B_0(t,m^2,m^2)$ function. This expression of the two-point function obtained by applying the expansion by regions method up to $\mathcal{O}(\lambda_R)$ is equal to the Taylor expansion of the exact result of $B_0(t,m^2,m^2)$.

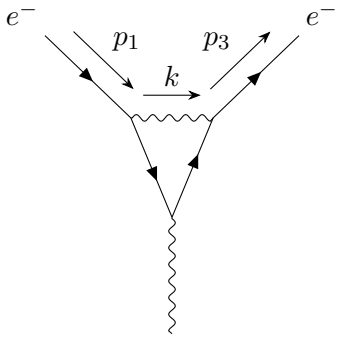

Figure 4.2: $C_0(m^2, m^2, t, m^2, 0, m^2)$ diagrammatic expression

4.2.2 $C_0(m^2, m^2, t, m^2, 0, m^2)$

The expansion of the Passarino-Veltman function C_0 is more complicated. We will introduce a different notation which is usually used in SCET theory [72]. The function $C_0(m^2, m^2, t, m^2, 0, m^2)$ is represented by the diagram in fig. 4.2 and it reads

$$C_0(m^2, m^2, t, m^2, 0, m^2) = \frac{\mu^{2\epsilon}}{i\pi^2} \int d^d k \frac{1}{k^2[(k+p_1)^2 - m^2][(k+p_3)^2 - m^2]}, \tag{4.12}$$

where $d = 4 - 2\epsilon$. We also define $Q^2 \equiv -(p_1 - p_3)^2 = -t$. The goal is to calculate this integral in the limit $p_1^2 \sim p_3^2 << Q^2$ that is, in the case in which the external legs carrying momenta p_1 and p_3 have small invariant masses.

We choose two light-like reference vectors in the direction of the momenta p_1 and p_3, in the frame in which $\vec{Q} = 0$:

$$n_\mu = (1, 0, 0, 1) \quad \text{and} \quad \bar{n}_\mu = (1, 0, 0, -1). \tag{4.13}$$

Then it is easy to prove the relations

$$n^2 = \bar{n}^2 = 0 \quad \text{and} \quad n \cdot \bar{n} = 2. \tag{4.14}$$

Any vector can be then decomposed in a component proportional to n, one proportional to $\bar{n}$ and a remainder perpendicular to both

$$p^\mu = (n \cdot p)\frac{\bar{n}^\mu}{2} + (\bar{n} \cdot p)\frac{n^\mu}{2} + p_\perp^\mu \equiv p_+^\mu + p_-^\mu + p_\perp^\mu. \tag{4.15}$$

The vector expressed in this light-cone components is useful to organize the expansion, since each component scales differently. Then the square of the momentum p and the scalar product of two different vectors p and q read

$$\begin{aligned} p^2 &= (n \cdot p)(\bar{n} \cdot p) + p_\perp^2, \\ p \cdot q &= p_+ \cdot q_- + p_- \cdot q_+ + p_\perp \cdot q_\perp. \end{aligned} \tag{4.16}$$

From now on we will express four vectors with the following notation

$$p^\mu = (n \cdot p, \bar{n} \cdot p, p_\perp) = (p_+, p_-, p_\perp). \tag{4.17}$$

From the relations in eq. 4.14, it is easy to show that $p_+^2 = 0$ and $p_-^2 = 0$. However one has to pay attention on this notation because the scalar quantities $p_+ \equiv n \cdot p$ and $p_- \equiv \bar{n} \cdot p$ should not be mixed up with the related vector quantities $p_\pm^\mu$ introduced above.

Similarly to the $B_0(t, m^2, m^2)$ computation, the expansion parameter, which vanishes in the limit we are interested in, is $\lambda_R = \frac{p_1^2}{Q^2} = \frac{p_3^2}{Q^2} = \frac{m^2}{-t}$.
We choose the reference vectors in the directions of large momentum flow $p_1^\mu \approx Q\frac{n^\mu}{2}$ and $p_3^\mu \approx Q\frac{\bar{n}^\mu}{2}$

and we also choose n^μ ($\bar{n}^\mu$) such that the perpendicular components of p_1^μ (p_3^μ) are zero. So the four vectors p_1^μ and p_3^μ will be

$$p_1^\mu \sim (1, \lambda_R, 0)Q \quad \text{and} \quad p_3^\mu \sim (\lambda_R, 1, 0)Q. \tag{4.18}$$

When computing the loop diagrams with the expansion by regions method, it is possible to show that only scalings $k^\mu \sim (\lambda_R^a, \lambda_R^b, \lambda_R^c)Q$, with $a + b = 2c$ and k the loop momentum, are important. For $c > 0$, these describe particles which go on shell as $\lambda_R \to 0$. Once we introduced this notation and the consideration necessary to describe our process, there are four regions that give non-vanishing contributions:

- Hard region: the components of the integration momentum scale as $k^\mu = (1, 1, 1)Q$. Then the denominators in eq. 4.12 become

$$\begin{aligned} k^2 &\sim \mathcal{O}(1), \\ (k+p_1)^2 - m^2 &= \underset{\mathcal{O}(1)}{k^2} + \underset{\mathcal{O}(1)}{2k_- \cdot p_{1,+}} + \underset{\mathcal{O}(\lambda_R)}{2k_+ \cdot p_{1,-}} \\ &= k^2 + 2k_- \cdot p_{1,+}\left(1 + \frac{2k_+ \cdot p_{1,-}}{k^2 + 2k_- \cdot p_{1,+}}\right), \\ (k+p_3)^2 - m^2 &= \underset{\mathcal{O}(1)}{k^2} + \underset{\mathcal{O}(\lambda_R)}{2k_- \cdot p_{3,+}} + \underset{\mathcal{O}(1)}{2k_+ \cdot p_{3,-}} \\ &= k^2 + 2k_+ \cdot p_{3,-}\left(1 + \frac{2k_- \cdot p_{3,+}}{k^2 + 2k_+ \cdot p_{3,-}}\right), \end{aligned} \tag{4.19}$$

  and the integral in eq. 4.12 reads

$$I_h = \frac{\mu^{2\epsilon}}{i\pi^2}\int d^dk \frac{1}{k^2(k^2 + 2k_- \cdot p_{1,+})(k^2 + 2k_+ \cdot p_{3,-})}\left(1 - \frac{2k_+ \cdot p_{1,-}}{k^2 + 2k_- \cdot p_{1,+}}\right)\left(1 - \frac{2k_- \cdot p_{3,+}}{k^2 + 2k_+ \cdot p_{3,-}}\right). \tag{4.20}$$

- Collinear region: the loop momentum k scales as $k^\mu \sim (1, \lambda_R, \sqrt{\lambda_R})Q$, and therefore we obtain

$$\begin{aligned} k^2 &\sim \mathcal{O}(\lambda_R), \\ (k+p_1)^2 - m^2 &= \underset{\mathcal{O}(\lambda_R)}{k^2} + \underset{\mathcal{O}(\lambda_R)}{2k_+ \cdot p_{1,-}} + \underset{\mathcal{O}(\lambda_R)}{2k_- \cdot p_{1,+}} = k^2 + 2k \cdot p_1, \\ (k+p_3)^2 - m^2 &= \underset{\mathcal{O}(\lambda_R)}{k^2} + \underset{\mathcal{O}(1)}{2k_+ \cdot p_{3,-}} + \underset{\mathcal{O}(\lambda_R^2)}{2k_- \cdot p_{3,+}} \\ &= 2k_+ \cdot p_{3,-}\left(1 + \frac{k^2}{2k_+ \cdot p_{3,-}} + \mathcal{O}(\lambda_R^2)\right). \end{aligned} \tag{4.21}$$

  So the integral reads

$$I_c = \frac{\mu^{2\epsilon}}{i\pi^2}\int d^dk \frac{1}{k^2(k^2 + 2k \cdot p_1)(2k_+ \cdot p_{3,-})}\left(1 - \frac{k^2}{2k_+ \cdot p_{3,-}} + \mathcal{O}(\lambda_R^2)\right). \tag{4.22}$$

- Anticollinear region: the momentum k scales as $k^\mu \sim (\lambda_R, 1, \sqrt{\lambda_R})Q$. The calculation of this integral is identical to the one performed in the collinear region if one makes the substitutions $p_1 \to p_3$ and $p_{3,-} \to p_{1,+}$ in eq. 4.22.

- Soft region: k scales as $k^\mu \sim (\lambda_R, \lambda_R, \lambda_R)Q$. The expansion of the propagator denominators takes the form

$$\begin{aligned} k^2 &\sim \mathcal{O}(\lambda_R^2), \\ (k+p_1)^2 - m^2 &= \underset{\mathcal{O}(\lambda_R^2)}{k^2} + \underset{\mathcal{O}(\lambda_R^2)}{2k_+ \cdot p_{1,-}} + \underset{\mathcal{O}(\lambda_R)}{2k_- \cdot p_{1,+}} = 2k_- \cdot p_{1,+} + \mathcal{O}(\lambda_R^2), \\ (k+p_3)^2 - m^2 &= \underset{\mathcal{O}(\lambda_R^2)}{k^2} + \underset{\mathcal{O}(\lambda_R)}{2k_+ \cdot p_{3,-}} + \underset{\mathcal{O}(\lambda_R^2)}{2k_- \cdot p_{3,+}} = 2k_+ \cdot p_{3,-} + \mathcal{O}(\lambda_R^2). \end{aligned} \tag{4.23}$$

Then the integral reads

$$I_s = \frac{\mu^{2\epsilon}}{i\pi^2}\int d^dk \frac{1}{k^2(2k_-\cdot p_{1,+})(2k_+\cdot p_{3,-})}. \tag{4.24}$$

It is possible to prove that this integral is vanishing both by applying the Feynman parameter or by involving integration by parts identities.

All of the other possible scalings of the integration momentum, of the form $k^\mu \sim (\lambda_R^a, \lambda_R^b, \lambda_R^c)Q$ and with a, b, c not matching one of the four cases listed above, give rise to scaleless integrals after the expansion, and therefore they do not contribute to the final result.

The $\mathcal{O}(1)$ contribution can be computed by introducing the usual Feynman parametrization, by using the relations $p_{1,-}^2 = p_{3,+}^2 = 0$ and $2p_{1,-}\cdot p_{3,+} = Q^2 = -t$ and then by integrating, following the formulae in App. A.3. We will sketch here the results of the integrals in the different regions:

- Hard region:

$$\begin{aligned} I_{h,0} &= \frac{\mu^{2\epsilon}}{i\pi^2}\int d^dk \frac{1}{k^2(k^2+2k_-\cdot p_{1,+})(k^2+2k_+\cdot p_{3,-})} \\ &= \frac{\mu^{2\epsilon}}{\pi^\epsilon}\frac{\sqrt{\pi}4^\epsilon}{(-t)^{\epsilon+1}}\frac{\Gamma(1+\epsilon)\Gamma(-\epsilon)}{\epsilon\Gamma(\frac{1}{2}-\epsilon)}. \end{aligned} \tag{4.25}$$

- Collinear region:

$$\begin{aligned} I_{c,0} &= \frac{\mu^{2\epsilon}}{i\pi^2}\int d^dk \frac{1}{k^2(k^2+2k\cdot p_1)(2k_+\cdot p_{3,-})} \\ &= \frac{\mu^{2\epsilon}}{\pi^\epsilon}\Gamma(1+\epsilon)\frac{(-\lambda_R t)^{-\epsilon}}{2t\epsilon^2}. \end{aligned} \tag{4.26}$$

- Anticollinear region:

$$I_{ac,0} = I_{c,0}. \tag{4.27}$$

- Soft region:

$$I_s = 0. \tag{4.28}$$

The final $\mathcal{O}(1)$ expansion of the C_0 function is obtained by summing all the contributions coming from the different regions and expanding the expression in $\epsilon \to 0$:

$$C_0(\mathcal{O}(1)) = \frac{1}{t}\left[(\Delta - \ln(-t))\ln(\lambda_R) - \frac{1}{2}\ln^2(\lambda_R) - \frac{\pi^2}{6}\right], \tag{4.29}$$

where the $\frac{1}{\epsilon}$ prescription, which is included in the Δ variable, identifies the IR divergences in dimensional regularization since the C_0 function is UV finite.
This result is perfectly consistent with the $\mathcal{O}(1)$ expansion in λ_R of the exact expression of the C_0 function.

Another method to compute the integrals in the different regions is based on integration-by-parts (IBP) reduction for multiloop integrals which exploits the IBP identities between integrals [73,74]. In order to apply the IBP reduction, the Mathematica *LiteRed* package is used [75,76]: at first stage it tries to find symbolic reduction rules using heuristics; then it applies the rules to the specific reduction. In our specific case we will use this Mathematica package to perform the computation at $\mathcal{O}(\lambda_R)$ of the C_0 function, since the integrals in this case can not be easily computed with the method applied at $\mathcal{O}(1)$. In fact, thanks to the IBP reduction method, the three-point functions in the hard and collinear regions can be written in terms of one- or two-point functions, the so called master integrals.

As a first step to compute the $\mathcal{O}(\lambda_R)$ contribution, we have to include the terms of the same order in the kinematics and this brings to the re-definition of the scalar product between the external momenta:

$$2p_{1,+}\cdot p_{3,-} = 2m^2 - t = -t\,(1+\lambda_R)\,, \tag{4.30}$$

where $\lambda_R = \frac{m^2}{-t}$ as usual. By computing the $\mathcal{O}(1)$ with *LiteRed*, we get the results (in terms of the master integrals):

- Hard region

$$I^{\lambda_R}_{h,0} = \frac{1-2\epsilon}{\epsilon t(1+2\lambda_R)} j(0,1,1), \tag{4.31}$$

where

$$\begin{aligned} j(0,1,1) &= \frac{\mu^{2\epsilon}}{i\pi^2}\int d^dk \frac{1}{(k^2+2k_-\cdot p_{1,+})(k^2+2k_+\cdot p_{3,-})} \\ &= \left(\frac{\mu^2}{\pi}\right)^{\epsilon}(2m^2-t)^{-\epsilon}\frac{\Gamma^2(1-\epsilon)\Gamma(\epsilon)}{\Gamma(2-2\epsilon)}. \end{aligned} \tag{4.32}$$

- Collinear region

$$I^{\lambda_R}_{c,0} = -\frac{(-1+\epsilon)}{2\epsilon t^2}\frac{1}{\lambda_R(1+2\lambda_R)} j(0,1,0), \tag{4.33}$$

where

$$\begin{aligned} j(0,1,0) &= \frac{\mu^{2\epsilon}}{i\pi^2}\int d^dk \frac{1}{(k^2+2k\cdot p_1)} \\ &= -\left(\frac{\mu^2}{\pi}\right)^{\epsilon}(m^2)^{-\epsilon+1}\Gamma(\epsilon-1). \end{aligned} \tag{4.34}$$

By expanding the results first for $\epsilon \to 0$ and then for $\lambda_R \to 0$, each integral in the different regions can be expressed as a sum of an $\mathcal{O}(1)$ term and an $\mathcal{O}(\lambda_R)$ "kinematical" correction coming from the re-definition of the scalar product shown above. By summing the contributions of the hard and (anti)collinear regions, the final expression is given by an $\mathcal{O}(1)$ contribution, which is exactly the result in eq. 4.29, plus an $\mathcal{O}(\lambda_R)$ correction given by

$$C_0^{\lambda_R}(\mathcal{O}(1)) = -\frac{2}{t}\lambda_R\left[\Delta - \ln(-t) + [\Delta - \ln(-t)]\ln(\lambda_R) - \frac{1}{2}\ln^2(\lambda_R) - \frac{2\pi^2}{3}\right]. \tag{4.35}$$

Apart from this, there is an $\mathcal{O}(\lambda_R)$ contribution coming from the λ_R-order integrand in the expansion of $C_0(m^2, m^2, t, m^2, 0, m^2)$ in the different regions (eq. 4.19 and eq. 4.21):

- Hard region

$$\begin{aligned} I_{h,\lambda_r} &= \frac{\mu^{2\epsilon}}{i\pi^2}\int d^dk \left[\frac{-2k_+\cdot p_{1,-}}{k^2(k^2+2k_-\cdot p_{1,+})^2(k^2+2k_+\cdot p_{3,-})} + \frac{-2k_-\cdot p_{3,+}}{k^2(k^2+2k_-\cdot p_{1,+})(k^2+2k_+\cdot p_{3,-})^2}\right] \\ &= \frac{2(-1+2\epsilon)}{t}\frac{\lambda_R}{(1+2\lambda_R)^2} j(0,1,1), \end{aligned} \tag{4.36}$$

where the master integral $j(0,1,1)$ is given in eq. 4.32.

- Collinear region

$$\begin{aligned} I_{c,\lambda_R} &= \frac{\mu^{2\epsilon}}{i\pi^2}\int d^dk \frac{-k^2}{k^2(k^2+2k\cdot p_1)(2k_+\cdot p_{3,-})^2} \\ &= -\frac{1}{t^2(1+2\lambda_R)^2} j(0,1,0), \end{aligned} \tag{4.37}$$

where the master integral $j(0,1,0)$ is given in eq. 4.34.

Now by expanding the results first for $\epsilon \to 0$ and then for $\lambda_R \to 0$, by summing the contributions coming from the different regions, we get

$$C_0^{\lambda_R}(\mathcal{O}(\lambda_R)) = \frac{2}{t}\lambda_R\left[1 - \ln(\lambda_R)\right]. \tag{4.38}$$

The final result of the $C_0(m^2, m^2, t, m^2, 0, m^2)$ is given by the sum of all the $\mathcal{O}(1)$ and $\mathcal{O}(\lambda_R)$ contributions:

$$\begin{aligned} C_0(m^2, m^2, t, m^2, 0, m^2) &= C_0(\mathcal{O}(1)) + C_0^{\lambda_R}(\mathcal{O}(1)) + C_0^{\lambda_R}(\mathcal{O}(\lambda_R)) \\ &= \frac{1}{t}\Bigg[[\Delta - \ln(-t)]\ln(\lambda_R) - \frac{1}{2}\ln^2(\lambda_R) - \frac{\pi^2}{6} \\ &\quad + 2\lambda_r\left(-\Delta + \ln(-t) + 1 - [1 + \Delta - \ln(-t)]\ln(\lambda_R) - \frac{1}{2}\ln^2(\lambda_R) + \frac{2\pi^2}{3}\right)\Bigg]. \end{aligned} \tag{4.39}$$

This expression of the three-point function obtained by applying the expansion by regions method, up to $\mathcal{O}(\lambda_R)$, is equal to the Taylor expansion of the exact result of $C_0(m^2, m^2, t, m^2, 0, m^2)$.

4.2.3 VP and vertex corrections expansion

As we said before, we will apply the expansion by regions method only to the vacuum polarization and vertex corrections. By recalling the expression of this two contributions in terms of the Passarino-Veltman functions (eq. 3.29 and eq. 3.32) we notice that the strategy of regions can be applied only to the corrections which involve the electron, namely the ones which contains the $B_0(t, m^2, m^2)$ and $C_0(m^2, m^2, t, m^2, 0, m^2)$ functions. Therefore we will expand the electron vacuum polarization correction and the electron vertex correction only.
The procedure that we will follow is: substitute in the amplitude the expression of the Passarino-Veltman functions obtained by the expansion by regions method; expand the result for $\lambda_R \to 0$.

- Electron vacuum polarization.

  The expression of the amplitude for this contribution, in terms of the Passarino-Veltman functions, is

$$\begin{aligned} \mathscr{X}_{VP}^{e^-} = Re\Bigg[&-\frac{64\pi\alpha^3}{3t^3}(2(m^2 + M^2 - s)^2 + 2st + t^2)\,(b_1(m) f B_0(t, m^2, m^2) \\ &- b_2(m) f B_0(0, m^2, m^2) + 2t\ln(m) - t)\Bigg], \end{aligned} \tag{4.40}$$

  where the coefficients $b_1(m)$ and $b_2(m)$ are defined in Sec. 3.5. The UV divergence has already been cancelled by the counterterm $\delta_3(m)$. Then we substitute the UV finite expression of B_0 obtained in eq. 4.11, namely we neglect the Δ term, and we expand for $\lambda_R \to 0$. The result at $\mathcal{O}(\lambda_R)$ reads:

$$\mathscr{X}_{VP}^{e^-} = Re\left[-\frac{64\pi\alpha^3}{3t^3}\left(e_1 + e_2\ln(\lambda_R) + 2\lambda_R\left(e_3\ln(\lambda_R) + e_4\right)\right)\right], \tag{4.41}$$

  where

$$\begin{aligned} e_1 &= 5\left[-2(M^2 - s)^2 - 2st - t^2\right], \\ e_2 &= 3\left[-2(M^2 - s)^2 - 2st - t^2\right], \\ e_3 &= 6t(M^2 - s), \\ e_4 &= 2t(5M^2 + 4s) + 18(M^2 - s)^2 + 9t^2. \end{aligned} \tag{4.42}$$

- Electron vertex.

  The amplitude expression of the electron vertex correction, coming from eq. 3.32, reads

$$\begin{aligned} \mathscr{X}_V = Re\Bigg[&\frac{16\pi\alpha^3}{t^2}(c_2 C_0(m^2, m^2, t, m^2, \lambda^2, m^2) + b_5 f B_0(0, m^2, m^2) \\ &+ b_6 f B_0(t, m^2, m^2) + a_1\ln(\lambda) + a_3\ln(m) + a_4)\Bigg], \end{aligned} \tag{4.43}$$

where the coefficients in front of the Passarino-Veltman functions are listed in Sec. 3.5. Since the expansion by regions method works in dimensional regularization, we have to replace the term proportional to the logarithm of the fictitious photon mass λ with the $\frac{1}{\epsilon}$ prescription. The two ways to express the IR divergences are bound by the relation [68]

$$\ln(\lambda) \to \frac{1}{2}\left[\frac{1-\gamma\epsilon-\epsilon\ln(\pi)}{\epsilon}+\ln(\mu^2)\right] \tag{4.44}$$

Once we have obtained an expression where the IR divergence is expressed in dimensional regularization we can substitute the expanded result of the Passarino-Veltman functions (4.10 and 4.39) in eq. 4.43. For the two-point function B_0 we neglect the UV divergent part, as we did for the VP amplitude, while in the three-point function we keep the IR divergent part, namely the Δ variable, since it can be cancelled by the introduction of the soft-Bremsstrahlung contribution, whose expansion is trivial. The last step is the expansion for $\lambda_R \to 0$.
Therefore the $\mathcal{O}(\lambda_R)$ electron vertex amplitude reads

$$\mathscr{X}_V = Re\left\{\frac{16\pi\alpha^3}{t^2}\left[f_1+f_2\ln(\lambda_R)+f_3\ln^2(\lambda_R)+\lambda_R\Big(f_4+f_5\ln(\lambda_R)+f_6\ln^2(\lambda_R)\Big)\right]\right\} \tag{4.45}$$

where

$$\begin{aligned}
f_1 &= -\frac{c_2}{t}\frac{\pi^2}{6} - b_5\ln(-t) + b_6\left(\Delta-\ln(-t)+2\right)+\frac{a_1}{2}\Delta + a_3\ln(-t)+a_4,\\
f_2 &= \frac{c_2}{2}\left(\Delta-\ln(-t)\right) - b_5 + a_3,\\
f_3 &= -\frac{c_2}{2t},\\
f_4 &= \frac{2c_2}{t}\left(-\Delta+\ln(-t)+1+\frac{2\pi^2}{3}\right) - 2b_6,\\
f_5 &= -\frac{2c_2}{t}\left(1+\Delta-\ln(-t)\right)+2b_6,\\
f_6 &= -\frac{c_2}{t},
\end{aligned} \tag{4.46}$$

where the coefficients c_2, b_5, b_6, a_1, a_3 and a_4 are listed in Sec.3.5.

The results obtained by applying the expansion by regions method to the electron VP and vertex correction to the μe scattering amplitude is equal to the result obtained by Taylor expanding the explicit expression of this contribution.

Chapter 5

Conclusions

The muon anomalous magnetic moment is a very well studied observable and its possible connection with New Physics kept it under close scrutiny in these last few years. In this thesis project we reviewed the state of the art of the SM theoretical prediction of the muon "g-2". We payed particular attention on the hadronic contribution because it is this contribution that dominates the uncertainty associated to the SM prediction.

The second step was the analysis of the LO and NLO muon-electron elastic scattering differential cross section. In particular we reproduced the explicit expression of the virtual corrections of the μe scattering cross section. These NLO contributions come from the vacuum polarization, the vertex correction and the box diagram. Moreover we were successful in reproducing the UV- and IR- finite result found in literature. We worked in dimensional regularization in order to regularize the ultraviolet divergences and we obtained the UV finite result in the on-shell renormalization scheme. We also find consistency with the soft-Bremsstrahlung contribution found in literature and we were able to obtain an IR finite result. All the results found for these virtual corrections were expressed in terms of the Passarino-Veltman functions and of kinematical variables. The computations were performed both by hands (vacuum polarization and vertex corrections) or by using the *FeynCalc* package of Mathematica.

The computation of the NLO differential cross section of the muon-electron elastic scattering was performed in the framework of the recent experimental proposal, MUonE, which aims at analyzing the scattering of high-energy muons on atomic electrons in order to measure the effective electromagnetic coupling $\Delta\alpha(q^2)$ for space-like four momentum transfers $q^2 = t < 0$.

In order to obtain a theoretical sensitivity which can be compared with the one that MUonE will reach, NLO QED corrections to the differential cross section are not enough; full NNLO QED corrections are necessary and up to now they are not yet known. Work is in progress to obtain this result using massless electrons and massive muons. In this thesis project we study a very powerful tool, based on the expansion by regions approach, to compute the electron mass effects in the NLO QED corrections.

The expansion by regions approach is a method of asymptotic expansion. The loop integrand can be simplified before integration by exploiting hierarchies of the parameters involved and expanding in powers of small parameter ratios. This method allows to treat all the singularities, that are found in the loop integral, properly. We applied the strategy of regions to the virtual corrections, in particular to the vacuum polarization and the vertex contributions. Since the parameter for which we performed the expansion by regions was the electron mass, we worked on the electron vacuum polarization and the electron vertex corrections specifically. The result that we obtained was UV-finite and gauge independent. The expression that we obtained by applying the expansion by regions method was successfully compared with the one coming from the Taylor expansion of the exact result for the muon-electron scattering differential cross section, obtained by standard methods. In particular we found that the two results were in agreement up to $\mathcal{O}(\lambda_R)$, where $\lambda_R = \frac{m^2}{-t}$, for both the electron vacuum polarization and the electron vertex corrections.

With this thesis project we showed that the results obtained by applying the expansion by regions method to the muon-electron scattering cross section at NLO in QED are equal to those obtained by Taylor expanding the exact expression of the observable of interest. This successful application of the expansion by region approach to the μe scattering will be important for future studies of the NNLO corrections, where the exact result is not yet known.

Appendix A

Reference formulae

A.1 Feynman rules

Starting from the QED Lagrangian

$$\mathscr{L} = -\frac{1}{4}(F_{\mu\nu})^2 + \bar{\psi}(i\partial\!\!\!/ - m)\psi - e\bar{\psi}\gamma^\mu\psi A_\mu, \tag{A.1}$$

the Feynman rules read

Dirac propagator :  $= \dfrac{i(\not{p} + m)}{p^2 - m^2 + i\epsilon}$, (A.2)

Photon propagator : 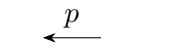 $= \dfrac{-ig_{\mu\nu}}{p^2 + i\epsilon}$, (A.3)

QED vertex : 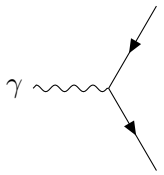 $= -ie\gamma^\mu$, (A.4)

External fermions : 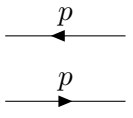
$= u^s(p) \quad (initial)$,
$= \bar{u}^s(p) \quad (final)$, (A.5)

External antifermions : 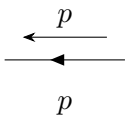
$= \bar{v}^s(p) \quad (initial)$,
$= v^s(p) \quad (final)$, (A.6)

External photons : 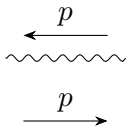
$= \epsilon_\mu(p) \quad (initial)$,
$= \epsilon^*_\mu(p) \quad (final)$, (A.7)

A.2 Trace technology

Traces of γ matrices can be evaluated as follows:

$$\begin{aligned} Tr(\mathbf{1}) &= 4, \\ Tr(\text{any odd \# of } \gamma'\text{s} &= 0, \\ Tr(\gamma^\mu\gamma^\nu) &= 4g^{\mu\nu}, \\ Tr(\gamma^\mu\gamma^\nu\gamma^\rho\gamma^\sigma) &= 4(g^{\mu\nu}g^{\rho\sigma} - g^{\mu\rho}g^{\nu\sigma} + g^{\mu\sigma}g^{\nu\rho}), \end{aligned} \tag{A.8}$$

Contractions of γ matrices with each other simplify to:

$$\begin{aligned}\gamma^\mu\gamma_\mu &= 4,\\ \gamma^\mu\gamma^\nu\gamma_\mu &= -2\gamma^\nu,\\ \gamma^\mu\gamma^\nu\gamma^\rho\gamma_\mu &= 4g^{\nu\rho},\\ \gamma^\mu\gamma^\nu\gamma^\rho\gamma^\sigma\gamma_\mu &= -2\gamma^\sigma\gamma^\rho\gamma^\nu.\end{aligned} \tag{A.9}$$

These identities apply in four dimension only.

A.3 Useful integrals

In this thesis project we often use the so called Feynman parameter and we perform the integration in d dimension of the loop momentum k. So in this section we list the useful formula applied.

- Feynman parameters

$$\frac{1}{A_1A_2...A_3} = \int_0^1 dx_1...dx_n\delta(\sum x_i - 1)\frac{(n-1)!}{[x_1A_1 + x_2A_2 + ... + x_nA_n]^n}. \tag{A.10}$$

  By repeated differentiation of eq. A.10, it is possible to obtain a more general formula

$$\frac{1}{A_1^{m_1}A_2^{m_2}...A_n^{m_n}} = \int_0^1 dx_1...dx_n\delta(\sum x_i - 1)\frac{\prod x_i^{m_i-1}}{[\sum x_iA_i]^{\sum m_i}}\frac{\Gamma(m_1 + ... + m_n)}{\Gamma(m_1)...\Gamma(m_n)}. \tag{A.11}$$

  The parametrization is slightly different if we consider propagators which are linear in k:

$$\frac{1}{A^aB^b} = \frac{\Gamma(a+b)}{\Gamma(a)\Gamma(b)}\int_0^\infty \frac{\beta^{b-1}}{(A+\beta B)^{a+b}}, \tag{A.12}$$

  where B is the linear propagator.

- Integrals in d dimension

$$\int d^dk\frac{1}{(k^2 + 2k\cdot Q - M^2)^\alpha} = (-1)^\alpha\frac{i\pi^{\frac{d}{2}}}{(M^2+Q^2)^{\alpha-\frac{d}{2}}}\frac{\Gamma(\alpha-\frac{d}{2})}{\Gamma(\alpha)}. \tag{A.13}$$

Appendix B

Scalar integrals

In this section we will list all the integrals which were necessary in this thesis project and we will sketch the procedure to solve them.

B.1 Passarino-Veltman integrals

The first kind of integrals we want to discuss are the Passarino-Veltman functions. We follow the notation in [68] and we work in the Bjorken-Drell metric so that $k^2 = k_0^2 - k_1^2 - k_2^2 - k_3^2$, where k is the loop momentum.
The generic expression for a one-loop integral is

$$\frac{\mu^{2\epsilon}}{i\pi^2}\int d^dk \frac{k^{\mu_1}\dots k^{\mu_n}}{D_0 D_1 \dots D_{n-1}}, \tag{B.1}$$

with $d = 4-2\epsilon$ and $D_i = (k+q_i)^2 - m_i^2 + i\epsilon$, while q_i are the internal momenta, related to the external ones p_i:

$$q_n \equiv \sum_{i=1}^{n} p_i \quad \text{and} \quad q_0 = 0. \tag{B.2}$$

The numerator of eq. B.1 can always be expressed in terms of the kinematic variables of the system considered and so the remaining integral can be written accordingly to the Passarino-Veltman notation:

$$\begin{aligned}
&A_0(m^2) = \frac{\mu^{2\epsilon}}{i\pi^2}\int d^dk \frac{1}{k^2 - m^2 + i\epsilon},\\
&B_0(p_1^2; m_1^2, m_2^2) = \frac{\mu^{2\epsilon}}{i\pi^2}\int d^dk \frac{1}{(k^2 - m_1^2 + i\epsilon)[(k+q_1)^2 - m_2^2 + i\epsilon]},\\
&C_0(p_1^2, p_2^2, p_3^2; m_1^2, m_2^2, m_3^2) = \frac{\mu^{2\epsilon}}{i\pi^2}\times\\
&\int d^dk \frac{1}{(k^2 - m_1^2 + i\epsilon)[(k+q_1)^2 - m_2^2 + i\epsilon][(k+q_2)^2 - m_3^2 + i\epsilon]},\\
&D_0(p_1^2, p_2^2, p_3^2, p_4^2; s_{12}, s_{23}; m_1^2, m_2^2, m_3^2, m_4^2) = \frac{\mu^{2\epsilon}}{i\pi^2}\times\\
&\int d^dk \frac{1}{(k^2 - m_1^2 + i\epsilon)[(k+q_1)^2 - m_2^2 + i\epsilon][(k+q_2)^2 - m_3^2 + i\epsilon][(k+q_3)^2 - m_4^2 + i\epsilon]},
\end{aligned} \tag{B.3}$$

where $s_{ij} = (p_i + p_j)^2$, μ is a scale introduced to preserve the natural dimensions of the integrals and the masses in the propagator are considered reals.
It is possible to prove that there are only four independent integrals in which the generic one-loop integral can be decomposed. For example the one-point function $A_0(m^2)$ can be written as

$$A_0(m^2) = m^2[1 + B_0(0; m^2, m^2)]. \tag{B.4}$$

So we are left with only the two-, three- and four-point functions.
The two-point function is easy to compute because, by using the Feynman parameters, it is possible to reduce the product of the two propagators to one single polynomial in the loop momentum. We recall the fact that the two-point function is UV divergent and IR finite.

Since the three-point function is more complicated we will sketch here the basic steps to perform this computation, following the procedure described in [67]. By introducing Feynman parameters we get

$$C_0 = i\pi^2 \int_0^1 dx \int_0^x dy[ax^2 + by^2 + cxy + dx + ey + f]^{-1}, \tag{B.5}$$

where the variables a, b, c, d, e and f are functions of the argument to which the C_0 function depends. After performing a suitable shift of y, in order to get rid of the x variable, the C_0 takes the form

$$C_0 = i\pi^2 \int_0^1 \frac{1}{P(y)} \ln \frac{Q(y)}{Q(y_0)}, \tag{B.6}$$

where $P(y)$ and $Q(y)$ are linear and quadratic polynomials in y respectively, and y_0 is a root of $P(y)$. Once we have obtained the structure of this C_0 function it is convenient to write it in terms of dilogarithms

$$Li_2(z) \equiv -\int_0^z \frac{\ln(1-t)}{t}. \tag{B.7}$$

We also recall that the three-point function is UV divergent and, in our specific case were an internal line is a photon (vertex correction), it is also IR divergent.

A similar approach can be applied to the four-point function, but in this case the computation is much more complicated, as shown in [67]. The result is expressed in terms of logarithms and dilogarithms as in the three-point function case.
Moreover we recall that the four-point function is UV finite while, in our case where the D_0 describe the box correction, it is IR divergence since there are two internal photon propagators.

B.2 Soft-Bremsstrahlung integrals

As we saw in Sec. 3.4, the soft-Bremsstrahlung contribution is of fundamental importance to cure the IR divergences of the muon-electron scattering virtual amplitude.
By computing this contribution, one encounters an integral that is essentially a phase space integral for photons with an energy less than some specified value ω_0. Here we will present the computation of this integral, by following the one performed in [67]. The integral to compute is

$$I(p_i, p_j) = \int_{|\mathbf{k}|<\omega_0} \frac{d^3k}{k_0} \frac{1}{(p_i \cdot k)(p_j \cdot k)}, \tag{B.8}$$

where $k_0 = \sqrt{\mathbf{k}^2 + \lambda^2}$, with λ the fictitious mass of the photon, $|\mathbf{k}| < \omega_0$ and p_i, p_j the four-momenta of the particles that emit the photon.
The case were $p_i = p_j$ is easy so we give here the result directly:

$$\begin{aligned} I(p,p) &= \int_{|\mathbf{k}|<\omega_0} \frac{d^3k}{k_0} \frac{1}{(p \cdot k)^2} \\ &= \frac{2\pi}{m^2}\left[\ln\left(\frac{2\omega_0}{\lambda}\right)^2 + \frac{E}{2|\mathbf{p}|}\ln\left(\frac{E-|\mathbf{p}|}{E+|\mathbf{p}|}\right)\right], \end{aligned} \tag{B.9}$$

where $E = \sqrt{|\mathbf{p}|^2 + m^2}$. For the case with $p_i \neq p_j$, the trick is to introduce a parameter ρ such that

$$I(p_i, p_j) = \rho \int_{|\mathbf{k}|<\omega_0} \frac{d^3k}{k_0} \frac{1}{(p \cdot k)(q \cdot k)}, \tag{B.10}$$

where $p = \rho p_i$ and $q = p_j$ and ρ is such that $(p-q)^2 = 0$. There will be two solutions and we will choose the one that gives the same sign to $p_0 - q_0$ as that of q_0.
Now we introduce the Feynman parameter x to combine the two factors in the denominator and to do the integral over $\mathbf{k}$.
Then by performing the following change of variables

$$\begin{aligned} u &= q + x(p-q), \\ l &= p_0 - q_0 = \pm|\mathbf{p}-\mathbf{q}|, \\ v &= \frac{p^2-q^2}{2l}, \end{aligned} \tag{B.11}$$

and by doing the integration in dx we obtain

$$\begin{aligned} I(p_i,p_j) = -\frac{2\pi\rho}{vl}\Bigg[&\frac{1}{2}\ln\frac{p^2}{q^2}\ln\left(\frac{2\omega_0}{\lambda}\right)^2 \\ &+\left\{\frac{1}{4}\ln^2\frac{u_0-|\mathbf{u}|}{u_0+|\mathbf{u}|} + \mathrm{Li}_2\left(\frac{v+u_0+|\mathbf{u}|}{v}\right) + \mathrm{Li}_2\left(\frac{v+u_0-|\mathbf{u}|}{v}\right)\right\}_{u=q}^{u=p}\Bigg], \end{aligned} \tag{B.12}$$

where $\rho = \frac{(p_i\cdot p_j)+\sqrt{(p_i\cdot p_j)^2-p_i^2p_j^2}}{p_i^2}$.
In the center of mass frame we have

$$\begin{aligned} p_{1,0} = p_{3,0} &= \sqrt{m^2 + \frac{\Lambda(s,m^2,M^2)}{4s}}, \quad |\mathbf{p_1}| = |\mathbf{p_3}| = \sqrt{\frac{\Lambda(s,m^2,M^2)}{4s}}, \\ p_{2,0} = p_{4,0} &= \sqrt{M^2 + \frac{\Lambda(s,m^2,M^2)}{4s}}, \quad |\mathbf{p_2}| = |\mathbf{p_4}| = \sqrt{\frac{\Lambda(s,m^2,M^2)}{4s}}, \end{aligned} \tag{B.13}$$

Then, for the different integrals obtained, we will have

- $I(p_1,p_3)$:

$$\begin{aligned} \rho_{13} &= \frac{(2m^2-t)+\sqrt{t^2-4m^2t}}{2m^2}, \\ v_{13} &= m^2\frac{\rho_{13}-1}{2l}, \quad l_{13} = (\rho_{13}-1)p_{1,0}. \end{aligned} \tag{B.14}$$

- $I(p_2,p_4)$:

$$\begin{aligned} \rho_{24} &= \frac{(2M^2-t)+\sqrt{t^2-4M^2t}}{2M^2}, \\ v_{24} &= M^2\frac{\rho_{24}-1}{2l}, \quad l_{24} = (\rho_{24}-1)p_{1,0}. \end{aligned} \tag{B.15}$$

- $I(p_1,p_4) = I(p_2,p_3)$:

$$\begin{aligned} \rho_{14} &= \frac{(m^2+M^2-u)+\sqrt{(m^2+M^2-u)^2-4m^2M^2}}{4m^2}, \\ v_{14} &= \frac{\rho_{14}m^2-M^2}{2l}, \quad l_{14} = \rho_{14}p_{1,0} - p_{4,0}. \end{aligned} \tag{B.16}$$

- $I(p_1,p_2) = I(p_3,p_4)$:

$$\begin{aligned} \rho_{12} &= \frac{(s-m^2-M^2)+\sqrt{\Lambda(s,m^2,M^2)}}{2m^2}, \\ v_{12} &= \frac{\rho_{12}m^2-M^2}{2l}, \quad l_{12} = \rho_{12}p_{1,0} - p_{2,0}. \end{aligned} \tag{B.17}$$

Bibliography

[1] H. N. Brown *et al.*, (Muon(g-2) Collaboration) *Phys. Rev.* D **62**, (2000) [091101]
H. N. Brown *et al.*, (Muon(g-2) Collaboration) *Phys. Rev. Lett.* **86**, (2001) [2227]
G. W. Bennet *et al.*, (Muon(g-2) Collaboration) *Phys. Rev. Lett.* **89**, (2002) [101804]
G. W. Bennet *et al.*, *Phys. Rev. Lett.* **89**, (2002) [129903]
G. W. Bennet *et al.* (Muon "g-2" Collaboration), *Phys. Rev. Lett.* **92**, 161802 (2004)
G. W. Bennet *et al.* (Muon "g-2" Collaboration), *Phys. Rev.* D **73**, 072003 (2006)

[2] B. Abi *et al.* (Muon "g-2" Collaboration), *Phys. Rev. Lett.* **126**, 14, 141801 (2021)

[3] T. Aoyama, *et al.*, *Phys. Rept.* **887**, 1-166 (2020)

[4] Sz. Borsanyi *et al.*, *Nature* **593**, 7857 (2021)

[5] N. Saito (J-Parc g-2/EDM Collaboration), *AIP Conf. Proc.* **1467**, 45 (2012)
T. Mibe (J-Parc g-2/EDM Collaboration), *Nucl. Phys. Proc. Suppl.* **218**, 242 (2011)
M. Abe *et al.*, *PTEP* **2019**, no.5 (2019)

[6] C. M. Carloni Calame, M. Passera, L. Trentadue and G. Venanzoni, *Phys. Lett* **B746**, 325 (2015)

[7] G. Abbiendi, *et al.*, *Eur. Phys. J. C.* **77**,3 (2017)
MuonE collaboration, *The MUonE Project*, *Letter of Intent* **CERN-SPSC-2019-026/SPSC-I-252** (2019)

[8] A. I. Nikishov, *Sov. Phys.* JETP **12**, 529 (1961)

[9] K. E. Eriksson, *Nuovo Cimento* **19**, 1029 (1961)

[10] K. E. Eriksson, B. Laesson and G. A. Rinander, *Nuovo Cimento* **30**, 1434 (1963)

[11] P. Van Nieuwenhuizen, *Nucl. Phys.* B **28**, 429 (1971)

[12] G. D'Ambrosio, *Lett. Nuovo Cim.* **38**, 593 (1983)

[13] T. V. Kukhto, N. M. Shumeiko and S. I. Timoshin, *J. Phys.* G **13**, 725 (1987)

[14] D. Yu. Bardin and L. Kalinovskaya, arXiv:hep-ph/9712310[hep-ph]

[15] N. Kaiser, *J. Phys.* G **37**, 115005 (2010)

[16] M. Alacevich, C. M. Carloni Calame, M. Chiesa, G. Montagna, O. Nicrosini and F. Piccinini, *JHEP* **02**, 155 (2019)

[17] P. Mastrolia, M. Passera, A. Primo and U. Schubert, *JHEP* **11**, 198 (2017)

[18] P. Mastrolia, M. Passera, A. Primo, U. Schubert and W. J. Torres Bobadilla, *EPJ Web COnf.* **179**, 01014 (2018)

[19] S. Di Vita, S. Laporta, P. Mastrolia, A. Primo and U. Schubert, *JHEP* **09**, 016 (2018)

[20] T. Engel, C. Gnendiger, A. Signer and Y. Ulrich, *JHEP* **02**, 118 (2019)

[21] A. A. Penin, *Phys. Rev. Lett.* **95**, 010408 (2005)

[22] A. Mitov and S. Moch, *JHEP* **05**, 001 (2007)

[23] T. Becher and K. Melnikov, *JHEP* **06**, 084 (2007)

[24] C. M. Carloni Calame, *et al.*, *JHEP* **11**, 028 (2020)

[25] Pulak Banerjee, T. Engel, A. Signer and Y. Ulrich, *SciPost Phys.* **9**, 027 (2020)

[26] R. Bonciani, A. Broggio, S. Di Vita, A. Ferroglia, M. K. Mandal *et al.*, arXiv:2106.13179 [hep-ph]

[27] M. Fael and M. Passera, *Phys. Rev. Lett* **122**, 19 (2019)

[28] M. Fael, *JHEP* **02**, 027 (2019)

[29] A. Masiero, P. Paradisi, M. Passera, *Phys. Rev.* D **102**, 7 (2020)

[30] P. S. Bhupal Dev, W. Rodejohann, X. Xu and Y. Zhang, *JHEP* **05**, 053 (2020)

[31] P. Banerjee, *te al.*, *Eur. Phys. J.* C **20**, 6 (2020)

[32] M. Beneke and V. A. Smirnov, *Asymptotic expansion of Feynman integrals near threshold*, *Nucl. Phys.* B **522**, 321-344 (1998)

[33] V. A. Smirnov, *Applied asymptotic expansions in momenta and masses*, *Springer Tracs Mod. Phys* **177**, 1-262 (2002)

[34] G. E. Uhlenbeck, S. Goudsmit, *Naturwissenschaften* **13**, 953 (1925) ; *Nature* **117**, 264 (1926)

[35] E. Back, A. Landé, *Zeemaneffekt und Multiplettstruktur der Spektrallinien*, 1st edn (J. Springer, Berlin 1925), pp 213

[36] W. Pauli, *Zeits. Phys.* **43**, 601 (1927)

[37] P. A. M. Dirac, *Proc. Roy. Soc.* A **117**, 610 (1928); A **118**, 351 (1928)

[38] J. E. Nafe, E. B. Nelson, I. I. Rabi, *Phys. Rev.* **71**, 914 (1947)

[39] P. Kusch, H. M. Foley, *Phys. Rev.* **73**, 421 (1948); *Phys. Rev.* **74**, 250 (1948)

[40] J. S. Schwinger, *Phys. Rev.* **73**, 416 (1948)

[41] G. F. Giudice, P. Paradisi and M. Passera, *JHEP* **11**, 113 (2012)

[42] M. Passera, *J. Phys.* G **31**, R75-R94 (2005)

[43] K. Melnikov and A. Vainshtein, *Theory of the muon anomalous magnetic moment*, Springer International Publishing (2006)

[44] F. Jegerlehner, *The anomalous magnetic moment of the muon*, Springer International Publishing (2017)

[45] T. Kinoshita, B. Nizic, Y. Okamoto, *Phys. Rev.* D **41**, 593 (1990)

[46] T. Kinoshita, W. J. Marciano, In: *Quantum Electrodynamics*, ed by T. Kinoshita (World Scientific, Singapore 1990) pp 419–478

[47] C. M. Sommerfield, *Phys. Rev.* **107**, 328 (1957);
C. M. Sommerfield, *Ann. Phys. NY* **5**, 26 (1958)

[48] A. Peterman, *Helv. Phys. Acta.* **30**, 407 (1957);
A. Peterman, *Nucl. Phys.* **5**, 667 (1958)

[49] J. A. Mignaco, E. Remiddi, *Nuovo Cim.* A **60**, 519 (1969);
R. Barbieri, E. Remiddi, *Phys. Lett.* B **49**. 468 (1974); *Nucl. Phys.* B **90**, 233 (1975);
R. Barbieri, M. Caffo, E. Remiddi, *Phys. Lett.* B **57**, 460 (1975);
M. J. Levine, E. Remiddi, R. Roskies, *Phys. Rev.* D **20**, 2068 (1979);
S. Laporta, E. Remiddi, *Phys. Lett.* B **265**, 182 (1991);

S. Laporta, *Phys. Rev.* D **47**, 4793 (1993); *Phys. Lett.* B **343**, 421 (1995);
S. Laporta, E. Remiddi, *Phys. Lett.* B **356**, 390 (1995)

[50] S. Laporta, E. Remiddi, *Phys. Lett.* B **379**, 283 (1996)

[51] S. Laporta, *Nuovo Cim.* A **106**, 675 (1993)

[52] S. Laporta, E. Remiddi, *Phys. Lett.* B **301**, 440 (1993)

[53] S. Laporta, *Phys, Lett.* B **772**, 232-238 (2017)

[54] R. H. Parker, C. Yu, W. Zhong, B. Estey and H. Muller, *Science* **360**, 191 (2018)

[55] A. Czarnecki, B. Krause and W. J. Marciano, *Phys. Rev.* D **52**, 2619 (1995)

[56] A. Czarnecki, B. Krause and W. J. Marciano, *Phys. Rev. Lett.* **76**, 3267 (1996)

[57] T. V. Kukhto, E. A. Kutaev, Z. K. Siligadze and A. Schiller, *Nucl. Phys.* B **371**, 567 (1992)

[58] C. Bouchiat and L. Michel, *J. Phys. Radium* **22**, 121 (1961)

[59] L. Durand, *Phys. Rev.* **128**, 441 (1962)
L. Durand, *Phys. Rev.* **129**, 2835 (1963)
S. J. Brodsky and E. de Rafael, *Phys. Rev.* **168**, 1620 (1962)
M. Gourdin and E. de Rafael, *Nucl. Phys.*B **10**, 667 (1969)

[60] B. E. Lautrup and E. de Rafael, *Phys.Rev.* **174**, 1835-1842 (1968)

[61] G. Backenstoss, B. D. Hyams, G. Knop, P. C. Martin and U. Stierlin, *Phys. Rev.* **129**, 2759 (1963)

[62] T. Kirk and S. Neddermeyer, *Phys. Rev.* **171**, 1412 (1968)

[63] P. L. Jain and N. J. Wixon, *Phys. Rev.* **23**, 715 (1969)

[64] V. Shtabovenko, R. Mertig and F. Orellana, *Comput. Phys. Commun* **256** (2020)

[65] V. Shtabovenko, R. Mertig and F. Orellana, *Comput. Phys. Commun* **207** (2016)

[66] R. Mertig, M. Bohm and A. Denner, *Comput. Phys. Commun.* **64**, 345-359 (1991)

[67] G. t' Hooft and M. Veltman, *Nucl. Phys.* B **153**, 365-401 (1979)

[68] R. Keith Ellis and G. Zanderighi, *JHEP* **02**, 002 (2008)

[69] W. Beenakker and A. Denner, *Nucl. Phys.* B **338**, 349-370 (1990)

[70] J. Bernabeu *et al.*, *Nucl. Phys.* B **790**, 160-174 (2008)

[71] A. Pak and A. Smirnov, *Eur. Phys. J. C.* **71**, 1626 (2011)

[72] T. Becher, A. Broggio and A. Ferroglia, *Lect. Notes Phys.* **896**, pp. 1-206 (2015)

[73] K. G. Chetyrkin and F. V. Tkachov, *Nucl. Phys.* B **192**, 159 (1981)

[74] F. V. Tkachov, *Phys. Lett.* B **100**, 65-68 (1981)

[75] R. N. Lee, *J. Phys, Conf. Ser* **523**, 012059 (2014)

[76] R. N. Lee, arXiv:hep-ph/1212.2685[hep-ph]